MODEL CATALYTIC STUDIES OF SINGLE CRYSTAL, POLYCRYSTALLINE METAL, AND SUPPORTED CATALYSTS

A Dissertation

by

ZHEN YAN

Submitted to the Office of Graduate Studies of
Texas A&M University
in partial fulfillment of the requirements for the degree of

DOCTOR OF PHILOSOPHY

December 2007

Major Subject: Chemistry

MODEL CATALYTIC STUDIES OF SINGLE CRYSTAL, POLYCRYSTALLINE METAL, AND SUPPORTED CATALYSTS

A Dissertation

by

ZHEN YAN

Submitted to the Office of Graduate Studies of
Texas A&M University
in partial fulfillment of the requirements for the degree of

DOCTOR OF PHILOSOPHY

Approved by:

Chair of Committee,	D. Wayne Goodman
Committee Members,	Michael P. Rosynek
	Daniel Shantz
	Manuel P. Soriaga
Head of Department,	David H. Russell

December 2007

Major Subject: Chemistry

ABSTRACT

Model Catalytic Studies of Single Crystal, Polycrystalline Metal, and Supported Catalysts. (December 2007)

Zhen Yan, B.S.; M.S., Peking University, China

Chair of Advisory Committee: Dr. D. Wayne Goodman

This dissertation is focused on understanding the structure-activity relationship in heterogeneous catalysis by studying model catalytic systems.

The catalytic oxidation of CO was chosen as a model reaction for studies on a variety of catalysts. A series of Au/TiO_2 catalysts were prepared from various metal-organic gold complexes. The catalytic activity and the particle size of the gold catalysts were strongly dependent on the gold complexes. The Au/TiO_2 catalyst prepared from a tetranuclear gold complex showed the best performance for CO oxidation, and the average gold particle size of this catalyst was 3.1 nm. CO oxidation was also studied over Au/MgO catalysts, where the MgO supports were annealed to various temperatures between 900 and 1300 K prior to deposition of Au. A correlation was found between the activity of Au clusters for the catalytic oxidation of CO and the F-center concentration in the MgO support.

In addition, the catalytic oxidation of CO was studied in a batch reactor over supported Pd/Al_2O_3 catalysts, a Pd(100) single crystal, as well as polycrystalline metals of rhodium, palladium, and platinum. A hyperactive state, corresponding to an oxygen-

covered surface, was observed at high O_2/CO ratios at elevated pressures. The reaction rate at this state was significantly higher than that on CO-covered surfaces at stoichiometric conditions. The oxygen chemical potential required to achieve the hyperactive state depends on the intrinsic properties of the metal, the particle size, and the reaction temperature.

A well-ordered ultra-thin titanium oxide film was synthesized on the Mo(112) surface as a model catalyst support. Two methods were used to prepare this Mo(112)-(8x2)-TiO_x film, including direct growth on Mo(112) and indirect growth by deposition of Ti onto monolayer SiO_2/Mo(112). The latter method was more reproducible with respect to film quality as determined by low-energy electron diffraction and scanning tunneling microscopy. The thickness of this TiO_x film was one monolayer and the oxidation state of Ti was +3 as determined by Auger spectroscopy, high-resolution electron energy loss spectroscopy, and X-ray photoelectron spectroscopy.

ACKNOWLEDGEMENTS

First I would like to thank my advisor, Dr. D. Wayne Goodman, for giving me the opportunity to pursue my Ph.D. and for his unfailing guidance and support throughout my graduate studies. I am also grateful to other committee members, Dr. Crooks, Dr. Ford, Dr. Rosynek, Dr. Shantz, and Dr. Soriaga, for their time and help.

I would like to thank all the group members for their assistance and support. Particularly, I thank Dr. Mingshu Chen for all the guidance and innumerable discussions we had over the last five years. I would also like to thank Dr. Fackler and Dr. Mohamed for providing me with the gold complexes, and Dr. Datye and Dr. Wang for the supported palladium catalysts.

Finally, thanks to my mother and father for their encouragement and to my wife for her love.

TABLE OF CONTENTS

LIST OF FIGURES

FIGURE Page

FIGURE Page

FIGURE Page

LIST OF TABLES

CHAPTER I

INTRODUCTION

Low Temperature CO Oxidation over Gold Catalysts

Although the early publications by Bond et al. [1, 2] and Parravano et al. [3, 4] reported that small gold particles exhibited catalytic activity for some reactions, such as hydrogenation of olefins and oxygen transfer reactions, gold was generally considered to be catalytically inactive [5]. Over the past twenty years, the volume of literature on the application of gold catalysts has been steadily increasing since Haruta reported that highly dispersed gold particles supported on metal oxides are very active for low-temperature CO oxidation [6, 7]. Studies on high surface area catalysts have shown that the catalytic performance of gold catalysts depends strongly on the size of the Au particles, with a maximum activity found for particles with an average diameter of ~3 nm [8]. Valden et al. found that the size dependence of CO oxidation on model catalysts is similar to that on high surface area catalysts, and explained this size dependence as arising from quantum size effects [9].

Many metal oxides have been investigated as support materials for gold catalysts. However, the results reported in the literature are often contradictory, and the role of the support is still under discussion. Behm and coworkers showed that the catalytic activity of gold catalysts was strongly dependent on the support materials [10]. They defined irreducible metal oxides such as Al_2O_3 and MgO as inert support materials, and

---

This dissertation follows the style of Journal of Catalysis.

reducible transition metal oxides, such as Fe_2O_3, NiO_x, CoO_x, and TiO_2, as active supports. However, Haruta et al. found no substantial differences in catalytic activity for gold supported on Al_2O_3, SiO_2, and TiO_2; instead they emphasized the moisture effect [11]. Recently, Overbury et al. synthesized uniformly sized Au nanoparticles (2–3 nm) on mesoporous TiO_2 and SiO_2 [12]. Much higher activity for CO oxidation was observed on Au/TiO_2 than on Au/SiO_2, indicating a strong support effect. Their results suggest that the presence of small Au particles (2–3 nm) alone is not sufficient to achieve high activity in CO oxidation.

For the preparation of highly dispersed gold catalysts, specific methods have been used, such as coprecipitation, deposition-precipitation, and chemical vapor deposition [13]. Conventional impregnation methods, which are widely used to prepare supported metal catalysts, were thought to be ineffective in producing active gold catalysts. Haruta reported that gold catalysts prepared by the impregnation method using $HAuCl_4$ as a precursor, had a particle size larger than 30 nm, and were catalytically inactive for CO oxidation [13].

Metal-organic and organometallic complexes have been widely used in the synthesis of catalysts, however, the use of metal-organic or organometallic gold complexes has been limited. Gates et al. reported that a supported mononuclear gold complex was active for ethylene hydrogenation at 353 K [14]. Recently, Iwasawa and coworkers [15-19] prepared highly active CO oxidation catalysts by grafting Au-phosphine complexes onto as-precipitated $Ti(OH)_4$. They found that the as-precipitated $Ti(OH)_4$ was essential for obtaining highly dispersed gold catalysts and the use of a

conventional TiO_2 support resulted in a much less active catalyst with a particle size greater than 15 nm. Previous work from our laboratories used a $[Au_6(PPh_3)_6](BF_4)_2$ complex to prepare Au catalysts by the impregnation method on a conventional TiO_2 support; the resulting catalyst was highly dispersed (< 5 nm) and active for CO oxidation [20].

In this dissertation, a series of Au/TiO_2 catalysts were prepared from precursors of various metal-organic gold complexes, and their catalytic activity for CO oxidation was studied [21]. The results are given in Chapter III.

Preferential Oxidation of CO (PROX)

A fuel cell is an electrochemical device that combines hydrogen and oxygen to produce electricity. The process is clean, quiet, much more efficient than internal combustion, and therefore, ideal for transportation applications. The most promising fuel cell technology for transportation applications is the polymer electrolyte membrane (PEM) fuel cell [22].

Hydrogen is the most efficient fuel for fuel cells. However, because hydrogen is a permanent gas, it is not practical to store sufficient hydrogen aboard a vehicle. As a result, fuel processing devices have been developed to generate hydrogen on board a vehicle [23]. In these fuel cell systems, methanol is converted to a hydrogen-rich gas by catalytic steam reforming and the water-gas shift reaction. The product stream contains approximately 45% H_2, 25% CO_2, 10% H_2O, 20% N_2, and 0.5–1% CO [22]. Even the small amount of CO severely degrades the Pt-based anode used in PEM fuel cells. For

the proper operation of PEM fuel cells, the CO concentration in the hydrogen feed must be kept below 20 ppm [22]. The preferential oxidation of CO (PROX) appears to be the most promising method for the purification of CO due to its simplicity and high efficiency.

In the early 1960s, Engelhard Industries developed a PROX process for ammonia synthesis gas plants [24]. About 2% of CO could be reduced to less than 10 ppm using a supported platinum catalyst. However, the catalyst becomes less effective in the presence of large amounts of CO_2 and H_2O. For fuel cell applications, recent efforts have focused on looking for new catalysts that are more effective than currently used Pt/Al_2O_3.

Oh and Sinketvitch [25] studied various noble metals and base metals for the PROX reaction. Ru/Al_2O_3 and Rh/Al_2O_3 were found to be the most active and selective catalysts for CO conversion in the presence of excess H_2. Compared to other platinum group metals, Pd/Al_2O_3 showed an unusual catalytic behavior, which was attributed to the change in the oxidation state of Pd.

Gold catalysts, due to their high activity for low-temperature CO oxidation, have also been studied for the PROX reaction [26, 27]. Haruta et al. reported that the CO conversion was higher than 95% at a temperature range from 323 to 353 K over Au/MnO_x catalysts for 1% CO in hydrogen [26]. Recently, Behm and coworkers studied the PROX reaction over a Au/Fe_2O_3 catalyst and found that the gold catalyst had comparable activity and selectivity to those of Pt/Al_2O_3 at considerable lower temperature [27].

Matralis and coworkers prepared a series of $CuO–CeO_2$ catalysts, which were very active and selective for the PROX reaction [28]. They also compared the performance of three different catalysts (i.e., Pt/Al_2O_3, Au/Fe_2O_3 and $CuO–CeO_2$) for the PROX reaction [29]. Although Au/Fe_2O_3 was the most active at relatively low reaction temperatures, $CuO–CeO_2$ was more active and selective than the others at higher reaction temperatures. Au/Fe_2O_3 lost a significant part of its activity under reaction conditions, whereas Pt/Al_2O_3 was the most resistant catalyst toward deactivation caused by CO_2 and H_2O.

The Role of Defects in Catalysis

It has been realized that many properties of solid materials are not controlled by their bulk structures, but by faults or defects in the structure [30, 31]. For example, the strength of a metal is frequently determined by linear defects called dislocations; the color of a gemstone is completely related to impurity atoms in the lattice. Even the electronic properties of the semiconductors in electronic devices are controlled by doping, a process of intentionally introducing impurities. Defects are also extremely important in many chemical processes, such as corrosion and catalysis. For these reasons, the study of the chemical, electrical, and optical properties of defects has attracted a continuously increasing interest.

Defects and catalysis

Experiments have shown that defective surfaces are often catalytically more active. Fox example, H_2 may dissociate at a single metal atom, or at step and kink sites on metal surfaces, but it may not readily dissociate on a smooth, highly coordinated (111) crystal face of platinum [32]. A stepped surface of Ni decomposes ethylene to smaller fragments at much lower temperatures (below 150 K), whereas the decomposition of ethylene on the Ni(111) face occurs at approximately 250 K [33-35].

In oxide materials, oxygen vacancies are the most common point defects [36], and often called color centers (F-centers) due to their specific optical absorption. Depending on the material, the structures and properties of oxygen vacancies can vary substantially. Examples of chemical reactivity closely related to the presence of oxygen vacancies have been reported for various oxides, such as TiO_2, SiO_2, and MgO [33-35]. For example, oxygen vacancies on TiO_2 surfaces play a critical role in the adsorption of O_2 because O_2 molecules seek the vacancy sites for non-dissociative adsorption, producing a superoxide species, O_2^-. This process occurs by the interaction of O_2 with surface Ti^{3+} sites, which are produced by thermal reduction of the surface [37].

Magnesium oxide is a particularly well-studied oxide because of the relatively simple structure of the MgO(100) surface [38-42]. A great effort has been made in recent years to characterize the MgO surface, and many different types of defects have been identified and described in the literature. Table 1 lists the most important point defects on MgO surfaces [43].

Table 1

Summary of most important point defects on MgO surfaces [43]

Defect	Symbol	Description
anion vacancy	F^{m+} (m = 0, 1, 2)	missing oxygen with trapped electrons
cation vacancy	V^{m-} (m = 0, 1, 2)	missing cation with holes at O neighbors
Mg and O divacancy	V_{MgO}	cation and anion vacancy
anion vacancy aggregate	M^{m+} (m = 0, 1)	aggregate of two or more O vacancies
low-coordinated cation	Mg^{2+}	coordinatively unsaturated cation
low-coordinated anion	O^{2-}	coordinatively unsaturated anion
hydroxy group	OH	proton attached to O^{2-}

According to the number of electrons (2, 1, or 0) trapped in the vacancy, oxygen vacancy is called F, F^+,or F^{2+} center [44]. F center is formed by the removal of a neutral O atom from a lattice, resulting in a cavity and two electrons. The two electrons are confined in the cavity region by the effect of the strong Madelung field. The removal of an O^+ ion, on the other hand, results in a single electron trapped in the cavity, leading to a paramagnetic F^+ color center. F and F^+ centers can be located in the bulk or on the surface of the material. In this latter case, the symbol F_s is used to distinguish the defect from its bulk.

The neutral F_s center, either alone or in association with an alkali ion impurity, is believed to contribute to the catalytic activity of MgO in some reactions [45]. Lunsford et al. reported the partial oxidation of methane to C_2 compounds over Li-promoted MgO, and suggested that the $[Li^+O^-]$ active centers might be formed from oxygen vacancies [46]. Tashiro et al. studied the oxidation of methane by N_2O on MgO, and found that the active oxygen species was O^-, which was formed from the reaction of N_2O with F_s^+ type centers [47].

It has been shown that F-centers on oxide surfaces are also the nucleation sites for metal clusters [48-51]. A scanning tunneling microscopy (STM) study by Besenbacher and coworkers showed that bridging oxygen vacancies on TiO_2 are the active nucleation sites for Au clusters [50]. They also found that a single oxygen vacancy can bind approximately three Au atoms. Sanchez et al. [51] reported that Au_8 clusters bound to F-centers on MgO are active for CO oxidation at temperatures as low as 140 K, whereas the same cluster on the defect-free MgO surface is catalytically inactive for CO oxidation.

Formation and detection of defects

Defects can be created by various types of high energy irradiations, including ultraviolet light, X-ray, electrons, and neutrons [41]. For example, Sibley and Chen found that the F-center production rate in MgO is a linear function of electron-irradiation intensity [52]. Thermal treatment can also produce defects. Wu et al. reported that three

types of defects, including F-centers were produced in ultrathin MgO films by annealing to temperatures higher than 1100 K [53].

Defects are often highly diluted, and therefore difficult to detect [43]. Electron paramagnetic resonance (EPR) spectroscopy, which measures the number of unpaired electrons in a solid, is an irreplaceable method in the study of defects. F^+ centers are paramagnetic, and thus can be detected by EPR. Another technique that has been widely used to characterize oxygen vacancies is optical spectroscopy. For example, F-centers in MgO cause a large absorption band at around 5 eV [54]. Recently, scanning tunneling microscopy (STM) has been used to study the formation of F-centers on MgO thin films [55, 56].

In this dissertation, CO oxidation was studied over Au/MgO catalysts where the MgO supports were annealed to various temperatures between 900 and 1300 K prior to deposition of Au. A correlation was found between the activity of Au clusters and the concentration of F-centers in the surface of the MgO support [57]. The results are given in Chapter IV.

Catalytic Oxidation of Carbon Monoxide

The oxidation of carbon monoxide is probably the most studied heterogeneous catalytic reaction due to its importance both in industry and in academic research. The oxidation of CO is one of the major reactions in automotive exhaust controls, and it also finds applications in fuel cells and CO_2 lasers [58]. CO oxidation is an ideal model

reaction for the study of surface-catalyzed reactions because it involves only diatomic molecules and presumably occurs over just a few elementary steps.

Many transition metals or their oxides have been found to catalyze the oxidation of CO, such as Cr, Mn, Fe, Co, Ni, Cu, and Ag [59, 60]. Platinum group metals, including Pt, Pd, and Rh, are the most widely used in industry due to their high activity and stability.

Mechanism

The oxidation of CO on single crystal surfaces of platinum group metals has been widely studied under ultrahigh vacuum (UHV) conditions [61, 62]. Significant progress has been made in understanding this prototypical reaction.

The mechanism of this reaction has been well summarized by Engel and Ertl [61]. On metal surfaces, the reaction is considered to follow a Langmuir-Hinshelwood (L-H) mechanism:

$$CO + * \rightarrow CO_{ad}$$

$$O_2 + 2* \rightarrow 2O_{ad}$$

$$O_{ad} + CO_{ad} \rightarrow CO_2 + 2*$$

Here, $*$ represents a free adsorption site on the metal surface. In this model, both oxygen and CO must be adsorbed on the surface before they can react with one another. Under typical reaction conditions, the surface is primarily covered by CO, and the reaction rate is determined by the CO desorption rate. The reaction is first-order with respect to

oxygen and negative first-order with respect to CO [63]. The observed activation energy is close to the adsorption energy of CO at the surface.

Another bimolecular model known as the Eley-Rideal (E-R) mechanism proposes the direct reaction of a gas phase molecule with an adsorbed one:

$$O_{ad} + CO \rightarrow CO_2$$

Early studies [64] seemed to favor the E-R mechanism; however, more detailed investigations [65] indicated that there was in fact no evidence for the E-R mechanism on Pt-group metals.

The oxidation of CO is generally considered as structure insensitive [63, 66], i.e. the catalytic activity is not influenced by surface structures. For example, the turnover rates on Pd particles between 1.5 and 8 nm were found to be virtually identical [66]. Thus, the results from single crystal studies can also be applied to polycrystalline real catalysts. However, at elevated pressures, the formation of surface oxides may play an important role. If surface oxidation does occur under certain conditions, it is reasonable to expect that the reaction rates and the mechanism on oxide surfaces will be different from those on metallic surfaces.

On ruthenium surfaces, some significant differences have been observed compared to other Pt-group metals (Rh, Pd, Pt, and Ir). Ruthenium is the most active at atmospheric pressure for CO oxidation [67, 68], but less active than other Pt-group metals under low pressure ($\sim 10^{-7}$ Torr) conditions [69]. The CO oxidation rate observed at atmospheric pressure is two to three orders of magnitude higher than that measured in

UHV. The high activity of Ru(0001) at elevated pressures was correlated with the presence of a monolayer of oxygen on the Ru surface [67].

Oscillatory reactions

In the early 1970s, Wicke and coworkers first reported rate oscillations in the catalytic oxidation of H_2 and CO [70]. Since then, oscillatory behavior has been observed in many heterogeneous catalytic reactions, including oxidation of H_2, CO, NH_3, or hydrocarbons, reduction of NO by CO or NH_3, as well as some hydrogenation reactions [71]. The most studied system exhibiting oscillatory behavior is the oxidation of CO on Pt-group metals. This system has been the subject of numerous theoretical and experimental studies, as well as several reviews [71-76]. The focus of recent studies has been to identify the cause of the oscillatory behavior.

Many mechanisms have been proposed to explain the rate oscillations during CO oxidation [75]. Among these mechanisms, the surface phase transition model and the oxidation-reduction model are often discussed in the literature and supported by experimental evidences.

Ertl and coworkers provided the evidence for the surface phase transition model on Pt(100) and Pt(110) surfaces [77-79]. These surfaces exhibit a reconstruction that can be reversibly lifted upon adsorption of CO. The different oxygen sticking coefficients of the two phases are responsible for the rate oscillations during the catalytic oxidation of CO. However, it has been suggested in the literature that such a mechanism is not responsible for rate oscillations at atmospheric pressure [80]. Furthermore, the

surface phase transition model cannot be applied to Pd since clean Pd surfaces do not reconstruct.

The oxidation-reduction model was first proposed by Sales, Turner, and Maple [81]. This model was successfully applied to Pd surfaces, which are different from Pt surfaces in that oxygen can penetrate into the Pd bulk and form subsurface oxygen. Subsurface oxygen species have been observed in CO titration experiments on Pd(110) [82]. The formation of subsurface oxygen can explain the oscillatory behavior. On the inactive CO-covered surface, the subsurface oxygen reservoir is depleted through segregation to the surface, followed by reaction with CO, thus restoring the catalytic activity of the clean Pd surface. With the active surface being covered by oxygen, the filling of the subsurface oxygen reservoir begins again, completing the oscillatory cycle. In this model, the catalyst surface is slowly deactivated by oxide formation and activated by reduction of this surface oxide.

The rate oscillations of CO oxidation on polycrystalline Pd, Ir, and Pt catalysts at atmospheric pressure have been attributed to the oxidation-reduction model [81]. In situ experiments have provided experimental evidences for this model [83, 84]. For example, in situ X-ray diffraction experiments showed that PtO and Pt_3O_4 were periodically formed on Pt/SiO_2 catalysts during rate oscillations at atmospheric pressure [83]. An in situ X-ray absorption spectroscopy (XAS) study showed a correlation between the change of the Pd K-edge position and the temperature oscillations during CO oxidation on supported Pd catalysts, and the change of the edge position corresponded to a periodic oxidation/reduction process [84].

Although the oscillatory behavior of CO oxidation has been studied extensively both experimentally and theoretically, this phenomenon is far from being fully understood. For example, the rate oscillations on Pt catalysts were explained by the surface phase transition model at low pressures and by the oxidation-reduction model at atmospheric pressure. It is still not clear if there is really a pressure at which the mechanism switches.

In this dissertation, the catalytic oxidation of CO was studied on various forms of Pt group metals, including single crystals, polycrystalline metals, and supported catalysts. A hyperactive state, corresponding to an oxygen-covered surface, was observed at high O_2/CO ratios at elevated pressures. The details of this study are given in Chapter V.

CHAPTER II

EXPERIMENTAL

Preparation and Characterization of Supported Gold Catalysts

Supported Au/TiO_2 and Au/MgO catalysts were prepared by incipient wetness impregnation using metal-organic gold complexes as precursors. Gold complexes with a varying number of gold atoms were used, including $[Au_2(dppm)_2](PF_6)_2$, $Au_3(Ph_2pz)_3$, $[Au_4(dppm)_2(3,5\text{-}Ph_2pz)_2](NO_2)_2$, and $Au_4(form)_4$, dppm = bis(diphenylphosphino) methane, form = (*p*-tolyl)NCN(*p*-tolyl). These complexes were provided by Dr. John P. Fackler in the Department of Chemistry at Texas A&M University [85, 86]. The amount of the particular gold complex was dissolved in CH_2Cl_2 or tetrahydrofuran (THF) and mixed with TiO_2 (Degussa P-25) or MgO (Fisher, Light) to obtain a nominal gold loading of 1 wt% with respect to the oxide support. The slurry was stirred at room temperature for ca. 1 h, heated on a hot plate to evaporate the solvent, and then vacuum dried overnight at 343 K. The as-synthesized catalyst was pretreated under different conditions. For Au/TiO_2, the as-synthesized sample was reduced in a hydrogen and helium mixture at 773 K for 3 h, followed by calcination in oxygen and helium at 673 K for 0.5 hours. For Au/MgO, the sample was pretreated in oxygen flow at 773 K for 3 hours. After pretreatment, the sample was cooled to the desired reaction temperature for activity measurements.

The TEM data were acquired on a high-resolution JEOL 2010 microscope at the University of New Mexico.

Continuous Flow Reaction System

The catalytic activity tests for Au/TiO_2 and Au/MgO were performed in a conventional flow reactor system. The catalyst (usually 50 mg) was placed in a fixed-bed quartz reactor and sandwiched between two layers of quartz wool. A K-type thermocouple was placed on the outside wall of the reactor in the middle of the catalyst. The reactor was heated by a furnace and the temperature was controlled by a temperature controller. For low temperature reactions, the reactor was immersed in a cold bath of water or acetone cooled by liquid nitrogen, and the temperature was then increased slowly.

CO (research purity, Matheson), O_2 (UHP, Matheson), H_2 (UHP, Matheson), and He (UHP, Matheson) were used in this study. The flow rates of these gases were controlled by mass flow controllers (Brooks, model 5850), and all reactions were carried out at atmospheric pressure. The reactant gas compositions were $CO/O_2/He = 1: 2: 25$ for the oxidation of CO, and $CO/O_2/H_2 = 1: 2: 50$ for the preferential oxidation (PROX) of CO. The total flow rates were 45 mL/min (GHSV = 54,000 mL/g/h) for CO oxidation and 84 mL/min (GHSV = 100,000 mL/g/h) for the PROX reaction. The products were analyzed by a Varian 3400 gas chromatograph (GC) equipped with a thermal conductivity detector (TCD) and a packed carbosphere column. CO conversion was calculated from GC peak areas of CO before and after the reaction, and it was in agreement with that calculated from CO_2 peaks. Reaction rates of CO oxidation, expressed as $mmol_{CO}/(g_{Au} \cdot s)$, were calculated from CO conversion, CO flowrate, and weight of gold.

Batch Reactor System

A stainless steel batch reactor was used to study the oxidation of CO as a function of O_2/CO ratio. A schematic diagram of the reactor system is shown in Fig. 1. The reactor system was equipped with two mechanic pumps and a turbomolecular pump (Balzers TPU 240), and had a base pressure of 3×10^{-8} Torr. The volume of the reactor was 0.51 L. A glass tube attached to the reactor can be used to trap CO_2 by immersing it in a liquid nitrogen bath. Powdered samples or metal wires were placed in a sample holder (1cm × 1cm), which was made of tantalum foil and spot-welded to two tantalum wires. Single crystal samples were directly mounted to tantalum wires. Samples or sample holders were heated resistively by a HP DC power supply and can go to 1300 K in vacuo. Sample temperature was measured by a C-type thermocouple (W-5%Re/W-26%Re) spot-welded to the back of sample holders or single crystals. Reaction temperature was monitored and controlled by a LabVIEW-based program.

Carbon monoxide was passed through a copper coil immersed in liquid nitrogen to remove metal carbonyls and other impurities. Oxygen (UHP, Matheson) was used as received without further purification. CO/O_2 gas mixtures with various ratios were prepared before the reaction to ensure complete mixing and were stored in glass bulbs. Reactant gas mixtures were introduced into the reactor through Nupro valves. Gas pressures were monitored by two MKS Baratrons (a 10 Torr differential pressure sensor and a 1000 Torr absolute pressure transducer), and were automatically recorded by the LabView program as a function of time. Most reactions were carried out at a total pressure of 5 to 10 Torr.

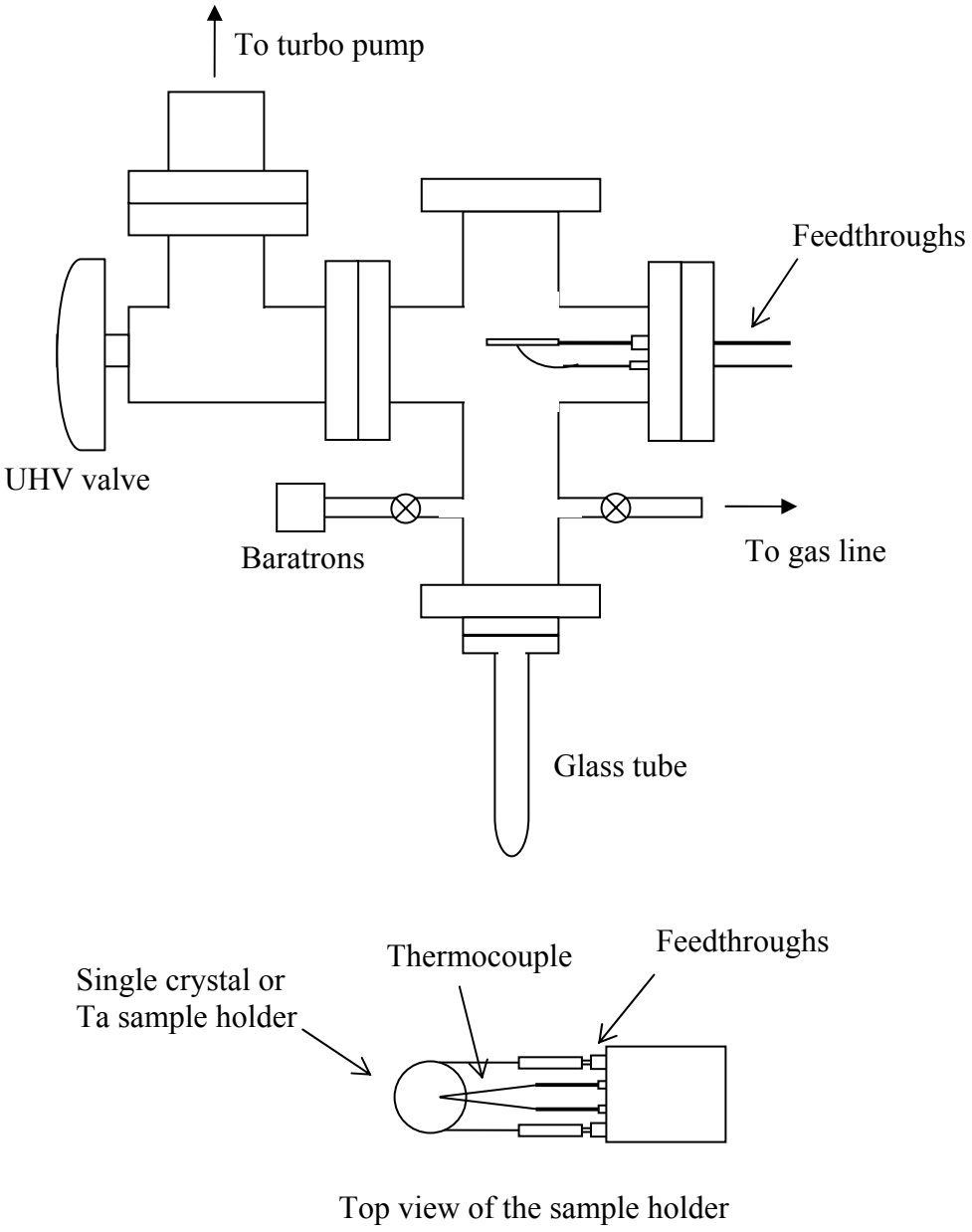

Fig. 1. Schematic of the batch reactor system.

For the oxidation of CO ($CO + ½ O_2 \rightarrow CO_2$), the total pressure of CO and O_2 decreases as the reaction proceeds and the reaction rate is proportional to the rate of pressure changes. Therefore, the reaction rate of CO oxidation can be calculated from the derivative of pressure with respect to reaction time:

CO_2 formation rate $\propto 2\ dP/dt$

Given the reactor volume V and the number of active sites, the CO_2 formation rate, defined as number of CO_2 molecules formed per surface metal atom per second or turnover frequency (TOF), can be calculated numerically:

$$TOF = 2 \times \frac{dP(Torr)}{760(Torr/atm)} \frac{V(L)}{(0.08206 L \cdot atm/mol \cdot K)(293K)} \frac{6.02 \times 10^{23}}{N} \frac{1}{dt(s)}$$

For single crystals, the number of active sites was calculated by the surface area and the atomic density of the crystal. For example, the number of active sites of the Pd(100) sample is 2.07×10^{15}. For polycrystalline wires, the reaction rate under stoichiometric conditions ($CO/O_2 = 2$) was measured first, and then divided by the reported TOF of the corresponding single crystal to give the number of active sites.

The O_2/CO ratios during reaction were calculated from the partial pressures of CO and O_2:

$p(CO) = p(CO, initial) - 2\Delta p$

$p(O_2) = p(O_2, initial) - \Delta p$

$p(CO, initial)$ and $p(O_2, initial)$ are the partial pressures of CO and O_2 before the reaction, and Δp is the change of total pressure (absolute value). The increase in total pressure

due to sample heating was usually small (~1% of the total pressure) and was calibrated using coefficients obtained from inert gases.

Pt Group Catalysts

The oxidation of CO was studied in the batch reactor on various forms of Pt group catalysts, including single crystals, polycrystalline metal wires, and supported catalysts.

The single crystal samples, including Pd(100) and Ru(0001), were cleaned by running CO oxidation reaction at 600 K in 1:1 CO/O_2 mixtures, followed by flash annealing to 1200–1300 K in vacuo [63, 87].

The following polycrystalline metal wires were used in this study:
Palladium (GoodFellow Cambridge Limited, 99.99+% purity, 0.25 mm diameter)
Rhodium (Johnson Matthey Inc., 99.9% purity, 0.25 mm diameter)
Platinum (Aldrich, 99.99% purity, 0.25 mm diameter).

The metal wires were etched in nitric acid, rinsed with doubly distilled water, and completely dried before placing in the sample holder. They were further cleaned in the reactor by running CO oxidation at 600 K in 1:1 CO/O_2 mixtures, followed by flash annealing to high temperatures in vacuo.

Three supported palladium catalysts were provided by Professor A. K. Datye at the University of New Mexico. The catalysts (7 wt% Pd/Al_2O_3) were prepared by impregnation of an aqueous solution of $Pd(NO_3)_2$ onto Al_2O_3, followed by drying and calcination at 873 K in air [88]. These catalysts underwent various sintering conditions,

and therefore had different particle size distributions. The average Pd particle sizes were 7, 13, and 30 nm for these three samples, respectively.

Another set of Pd/Al_2O_3 catalysts were provided by Dr. Chen-Bin Wang at National Defense University, Taiwan [89]. These samples were prepared by impregnation of H_2PdCl_4 solutions, followed by drying and calcination at 773 K in air.

CHAPTER III

CO OXIDATION OVER GOLD CATALYSTS PREPARED FROM METAL-ORGANIC GOLD COMPLEXES*

Au/TiO_2 Catalysts

The Au/TiO_2 catalysts were prepared from metal-organic gold complexes using the impregnation method as described in Chapter II. The catalysts prepared from $[Au_2(dppm)_2](PF_6)_2$, $Au_3(Ph_2pz)_3$, $[Au_4(dppm)_2(3,5\text{-}Ph_2pz)_2](NO_2)_2$, and $Au_4(form)_4$ are denoted as Au_2, Au_3, Au_4 #1, and Au_4 #2, respectively.

Fig. 2 shows the CO conversion as a function of reaction temperature over 1 wt% Au/TiO_2 catalysts prepared from various gold complexes. The two samples prepared from tetranuclear gold complexes were more active than those prepared from di- and tri-nuclear complexes. The Au_4 #1 and Au_4 #2 catalysts showed apparent CO oxidation activities at temperatures below 273 K, with the lowest temperature of CO oxidation observed at about 220 K over the Au_4/TiO_2 #1 sample. The room-temperature CO conversion over the Au_4 #1 sample was over 90%, whereas no reaction was observed over the Au_2 sample at the same temperature. The catalyst lifetime tests showed that the catalytic activities of the two Au_4/TiO_2 samples decreased slowly with time, with approximately 20% of their activities being lost in the first 4 hours at room temperature (Fig. 3).

---

*Reprinted with permission from "CO oxidation over Au/TiO_2 prepared from metal-organic gold complexes" by Z. Yan, S. Chinta, A. A. Mohamed, J. P. Fackler Jr., and D. W. Goodman, 2006. *Catalysis Letters*, 111, 15-18, Copyright [2006] by Springer Science and Business Media.

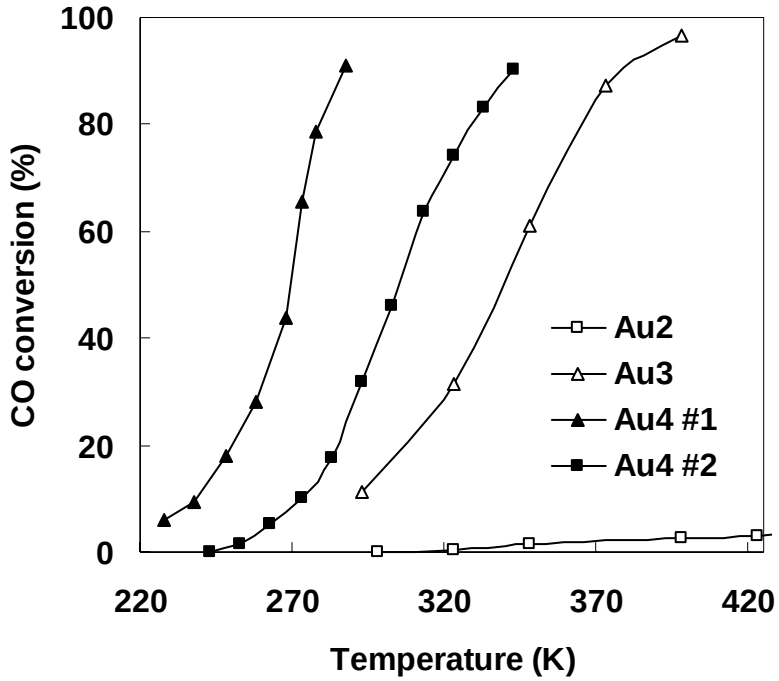

Fig. 2. CO conversion as a function of temperature over 1 wt% Au/TiO_2 catalysts. The data were measured in a mixture of $CO/O_2/He$ (1:2:25) with a GHSV of 54,000 $cm^3/g/h$.

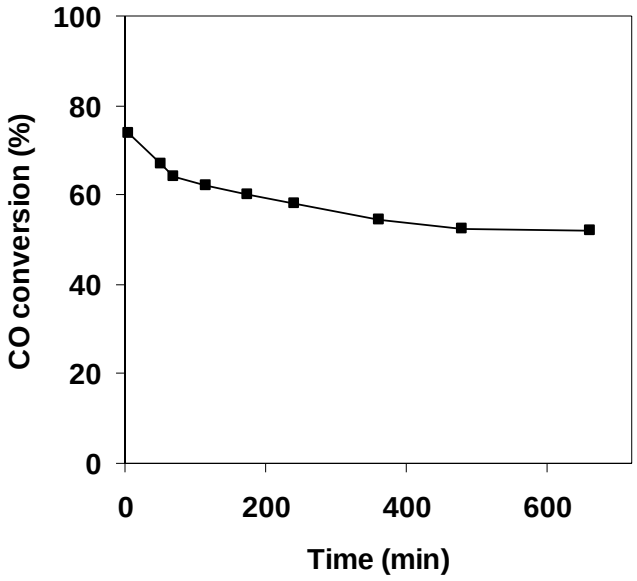

Fig. 3. CO conversion at room temperature as a function of time over the Au_4 #2 catalyst. The data were measured in a mixture of $CO/O_2/He$ (1:2:25) with a GHSV of 54,000 $cm^3/g/h$.

Fig. 4 shows the Arrhenius plots for CO oxidation over the Au/TiO_2 catalysts. The activation energies for these catalysts were between 18 and 37 kJ/mol, consistent with the literature values for CO oxidation over supported Au catalysts [90, 91]. The TEM image and the particle size distribution of Au_4/TiO_2 #1 are shown in Fig. 5. Most of the gold particles were in the range of 2–6 nm; the average Au particle diameter was 3.1 nm with a percent deviation of 40%. The average gold particle sizes of the Au_2, Au_3, and Au_4 #2 samples were 7.7, 4.8, and 3.0 nm, respectively.

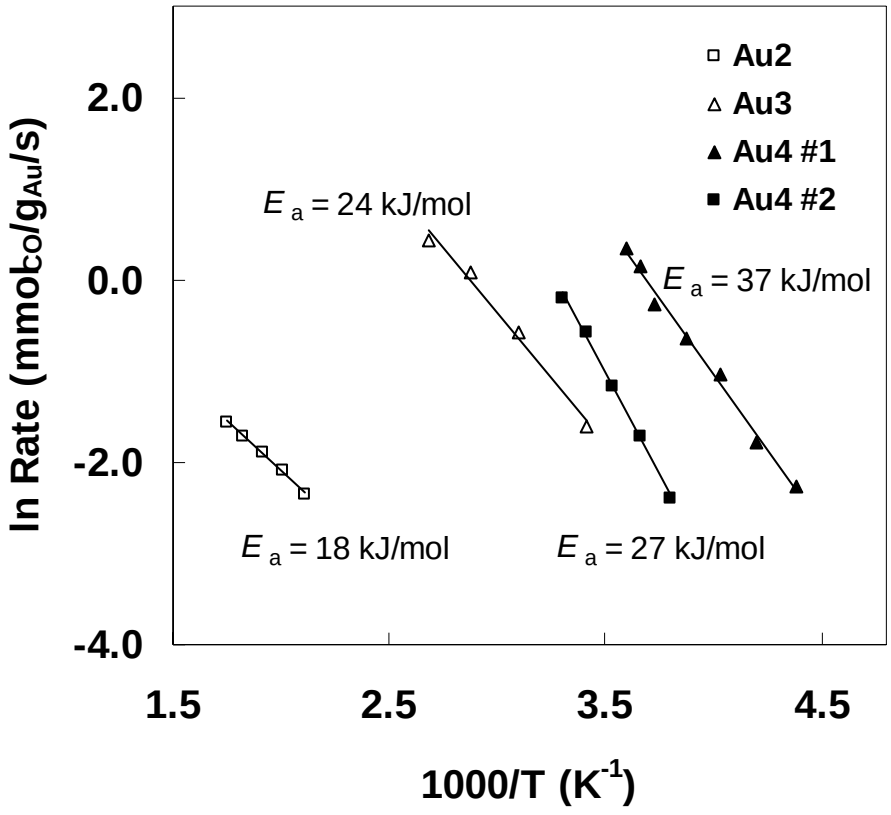

Fig. 4. Arrhenius plots for CO oxidation over Au/TiO_2 catalysts. The data were measured in a mixture of $CO/O_2/He$ (1:2:25) with a GHSV of 54,000 $cm^3/g/h$.

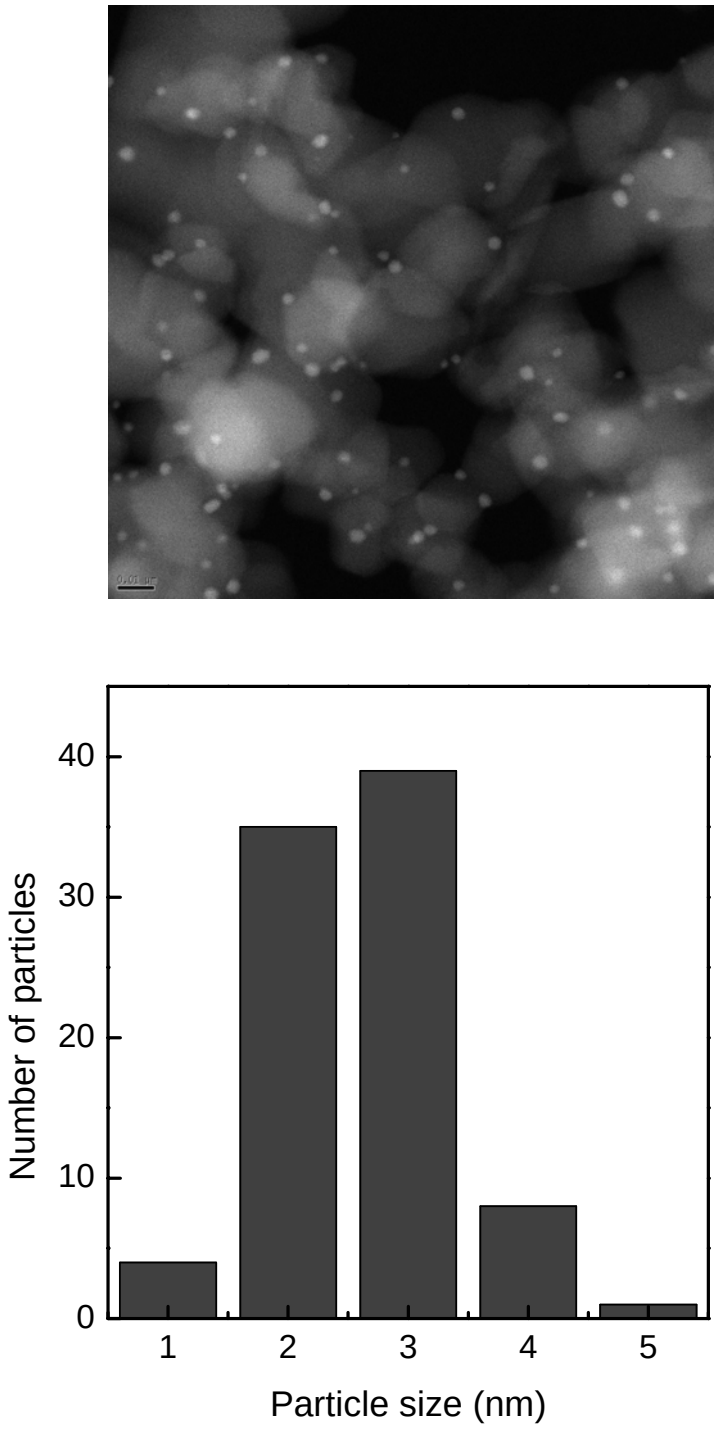

Fig. 5. TEM image and gold particle size distribution of Au_4 #1/TiO_2 catalyst.

The preferential oxidation (PROX) of CO in excess hydrogen was measured over the Au_4/TiO_2 #1 catalyst. Fig. 6 shows the CO conversion and CO_2 selectivity as a function of reaction temperature. At room temperature, CO conversion was approximately 54% and the selectivity for CO_2 was over 60%. As the reaction temperature increased, both CO conversion and CO_2 selectivity decreased; however, the CO_2 selectivity dropped more quickly. From room temperature to 325 K, CO conversion was almost constant, whereas CO_2 selectivity decreased from 62% to 23%.

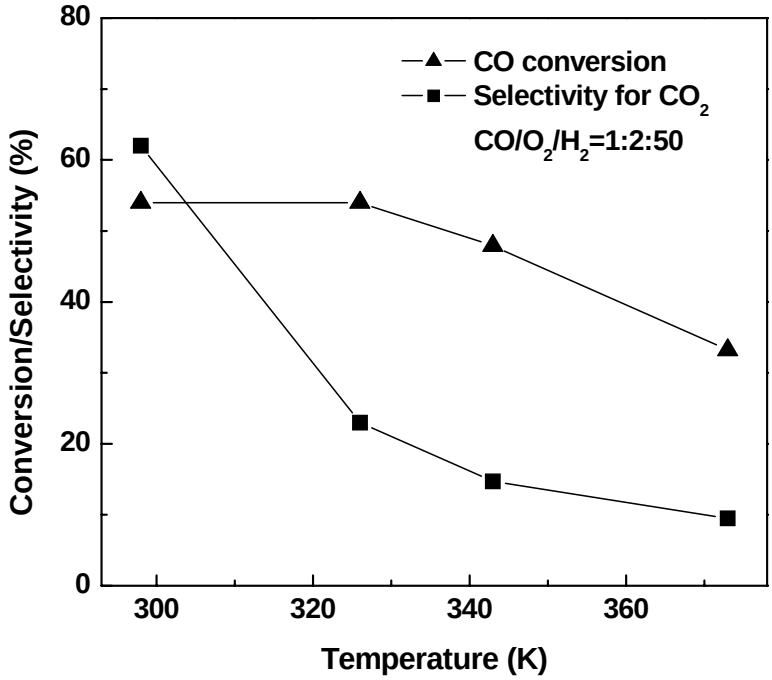

Fig. 6. Preferential oxidation of CO on Au_4 #1/TiO_2. The data were measured in a mixture of $CO/O_2/H_2$ (1:2:50) with a GHSV of 100,000 $cm^3/g/h$.

These data showed that Au/TiO_2 catalysts prepared from certain metal-organic gold complexes were highly active for CO oxidation. Using a particular precursor complex was critical to obtaining a highly active gold catalyst. Contrary to the assumptions by Haruta [13] and Iwasawa [15-19], our results indicated that a highly-dispersed gold catalyst can be prepared using the impregnation method and a conventional TiO_2 support.

Specific CO oxidation activities of Au/TiO_2 prepared by various methods are compared in Table 2. The Au/TiO_2 catalysts prepared from Au_4 complexes in this work showed similar activities as the gold catalysts prepared using the deposition-precipitation method, and were superior to those prepared by other methods.

Several factors may contribute to the high activity of our Au/TiO_2 catalysts. First, the use of metal-organic complexes as precursors avoided chloride. $HAuCl_4$ is widely used as a gold precursor in catalytic studies, invariably leaving a certain amount of chloride residue in the catalysts after preparation. Recently, both experimental and theoretical studies have shown that chloride can poison the catalytic performance of gold catalysts for CO oxidation. Oh et al. have shown that chloride residue on a catalyst can promote agglomeration of Au particles during heat treatment, and can inhibit the catalytic activity by poisoning the active site [92]. Density functional calculations show that chloride can act as a poison by weakening the adsorption of O_2 and lowering the stability of the $CO{\cdot}O_2$ intermediate complex [93]. Clearly metal-organic or organometallic precursors provide an attractive route for the preparation of chloride-free gold catalysts.

Table 2

Comparison of CO oxidation rates on Au/TiO_2 catalysts prepared by different methods

Gold Precursor	Catalyst	Prep.[a]	T (K)	Rate ($mmol/g_{Au}/s$)	Ref.
$HAuCl_4$	1% Au/TiO_2	IMP	300	2×10^{-5}	[8]
$HAuCl_4$	1% Au/TiO_2	FD	300	2×10^{-5}	[8]
$AuPPh_3NO_3$	3% Au/TiO_2	IMP	313	6×10^{-3}	[18]
$HAuCl_4$	1.7% Au/TiO_2	AuC	300	0.01	[94]
$HAuCl_4$	2.3% Au/TiO_2	IMP	313	0.05	[95]
$Me_2Au(acac)$	4.6% Au/TiO_2	CVD	262	0.05	[96]
$AuPPh_3NO_3$	3% $Au/Ti(OH)_4$	IOH	300	0.05	[18]
$Me_2Au(acac)$	2.4% Au/TiO_2	CVD	293	0.06	[96]
$HAuCl_4$	2.3% Au/TiO_2	DP	300	0.2	[8]
$Au_6(PPh_3)_6(BF_4)_2$	1% Au/TiO_2	IMP	293	0.3	[20]
$HAuCl_4$	3.1% Au/TiO_2	DP	300	0.6	[8]
$Au_4(form)_4$	1% Au/TiO_2	IMP	300	0.7	[b]
$[Au_4(dppm)_2(3,5\text{-}Ph_2pz)_2]_2(NO_3)_2$	1% Au/TiO_2	IMP	300	3	[b]

[a] IMP, impregnation of oxides; FD, photodecomposition; DP, deposition-precipitation; CVD, chemical vapor deposition.
[b] Present work.

Another explanation for the high activity of our Au/TiO_2 catalysts also relates to the use of metal-organic precursor complexes. Upon deposition onto the oxide support, these complexes interact with the surface OH groups and become less mobile compared to gold atoms deposited using $HAuCl_4$. Several studies have shown that metal-organic and organometallic complexes are capable of reacting directly with surface OH groups on inorganic oxide surfaces, such as SiO_2, Al_2O_3, and TiO_2, to form well-defined covalent bonds [97, 98]. The organic groups in metal complexes could be retained partially or completely following deposition onto oxide supports. For example, Iwasawa et al. showed that the cluster framework of $[Au_9(PPh_3)_8](NO_3)_3$ was virtually the same after attachment to TiO_2 [99]. This framework can inhibit agglomeration of gold particles during calcination. Altogether these factors prevent the sintering of gold, and the well-defined structures of the gold complexes lead to a narrow particle size distribution compared to the deposition-precipitation method.

Our results showed that the use of a specific gold precursor complex correlated directly with the gold particle sizes and the catalytic activity of the resulting catalysts. Gold complexes with varying charges and numbers of gold atoms yielded Au/TiO_2 catalysts with varying particle size distributions. The detailed relation between the nature of the precursor complex (number of gold atoms and electronic charge) and the activity of the resulting catalyst is a subject of ongoing investigation.

The Au/TiO_2 catalysts showed a potential application for the PROX reaction, which is used to remove trace amounts of CO from hydrogen for fuel cell applications. The most widely used PROX catalyst in industry is alumina-supported platinum, which

operates at 423–473 K [27, 100]. Recently, Behm and coworkers studied the PROX reaction over Au/Fe_2O_3 and found that the gold catalyst had comparable activity and selectivity to that of Pt/Al_2O_3 at considerably lower temperatures [27]. Recent theoretical studies showed that gold is more selective than Pt for the PROX reaction at low temperatures [101]. Our Au/TiO_2 catalysts exhibited comparable reaction rates and selectivities to those found for Au/Fe_2O_3 prepared by the coprecipitation method. Although the CO conversion is insufficient for application to fuel cells, the low-temperature activity of gold catalysts has distinct advantages over Pt-based catalysts.

Au–Ag Bimetallic Catalysts

Silver catalysts have been used for a number of partial oxidation reactions in industry, such as ethylene epoxidation and formaldehyde synthesis reactions [58]. Recently, silver catalysts have been studied as a possible substitute for precious metals in pollution control because they are more active than Pt-group metals at low temperatures and more stable than gold catalysts under reaction conditions [102-104]. Synergistic effects have been reported in CO oxidation over Au–Ag bimetallic catalysts, which showed higher activity than either of the pure metallic catalysts [105-107]. The catalytic activity of Au–Ag bimetallic catalysts for CO oxidation was investigated in an attempt to improve the activity and stability of gold catalysts, and the results are given in this section.

Ag-Au/TiO_2 catalysts were prepared from gold-silver mixed-metal complexes by the method described in Chapter II. The catalysts prepared from $[Ag(\mu\text{-}3,5\text{-}Ph_2pz)]_3$,

[Au(carb)Ag_2(μ-3,5-Ph_2pz)$_2$], and [Au_2(carb)$_2$Ag(μ-3,5-Ph_2pz)] [108, 109] are denoted as Ag/TiO_2, Ag_2-Au/TiO_2, and Ag-Au_2/TiO_2, respectively.

Fig. 7 shows the CO conversion as a function of temperature over two Au-Ag bimetallic catalysts. For comparison, the result for an Ag/TiO_2 catalyst is also shown in the figure. Both of the Ag-Au/TiO_2 samples showed room-temperature CO oxidation activity, and the lowest temperature of CO oxidation was observed at about 200 K over the Ag-Au_2/TiO_2 sample, which was very close to the activity of the Au_4 #1 catalyst (Fig. 2). $T_{50\%}$ (defined as the temperature at which the conversion of CO reaches 50%) on Ag-Au_2, Ag_2-Au, and Ag catalysts were 268, 293, and 438 K, respectively.

The activation energy (Fig. 8) and the deactivation curve (Fig. 9) of the Ag-Au_2 catalyst were also similar to those of the Au_4/TiO_2 catalysts. These results imply that gold was probably the only active component for CO oxidation in these Au-Ag bimetallic catalysts, and synergistic effects were not observed. This may suggest that gold and silver formed monometallic particles separately during calcinations, instead of forming alloy particles.

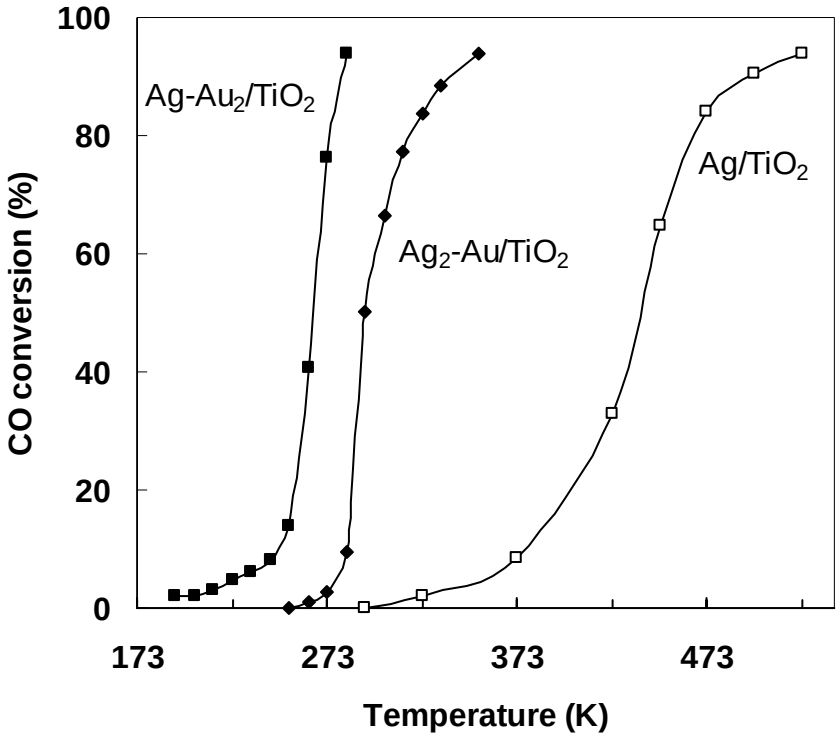

Fig. 7. CO conversion as a function of temperature over TiO_2 supported Ag-Au_2, Ag_2-Au, and Ag catalysts. The data were measured in a mixture of CO/O_2/He (1:2:25) with a GHSV of 54,000 $cm^3/g/h$.

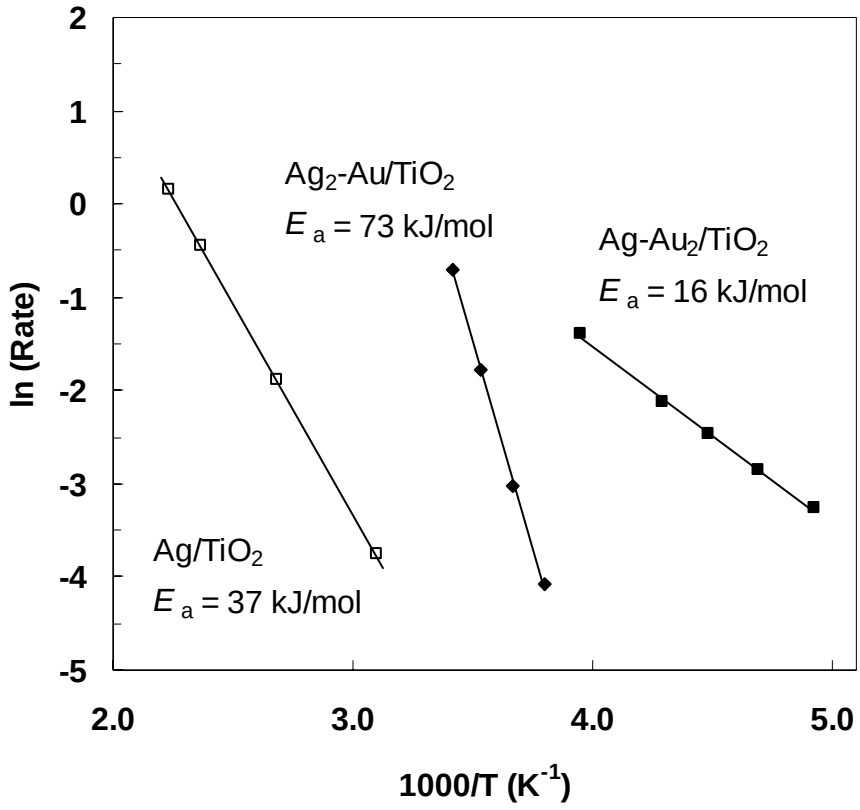

Fig. 8. Arrhenius plots for CO oxidation over TiO_2 supported Ag-Au_2, Ag_2-Au, and Ag catalysts. The data were measured in a mixture of CO/O_2/He (1:2:25) with a GHSV of 54,000 cm^3/g/h.

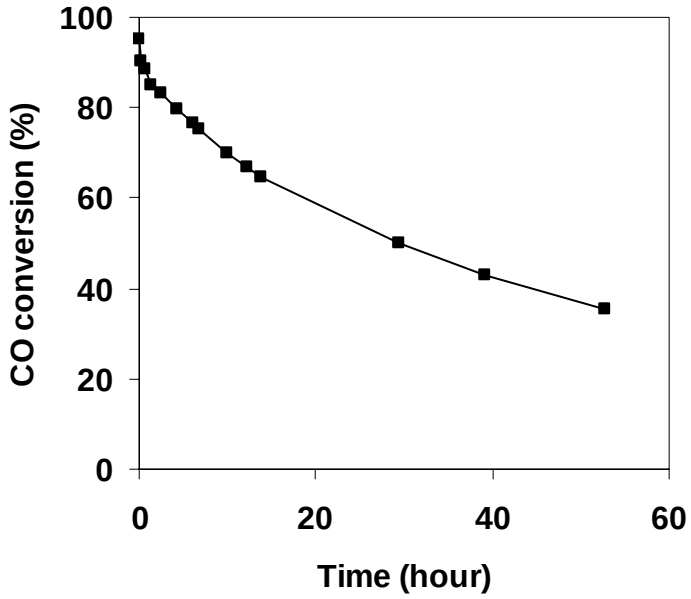

Fig. 9. CO conversion at room temperature as a function of time over the Ag-Au_2 catalyst. The data were measured in a mixture of CO/O_2/He (1:2:25) with a GHSV of 54,000 cm^3/g/h.

Conclusions

Our results showed that highly active Au/TiO_2 catalysts can be prepared from specific metal-organic gold complexes and a conventional TiO_2 support utilizing the impregnation method. The catalytic activity and the particle size of the gold catalysts strongly depend on the gold complexes, and the Au/TiO_2 with the maximum CO oxidation activity was prepared from a Au_4 complex. The Au/TiO_2 catalysts also showed promising results for the PROX reaction. The activities of the bimetallic Ag-Au/TiO_2 catalysts were similar to those of the Au_4/TiO_2 catalysts, and no synergistic effect was observed.

CHAPTER IV

CO OXIDATION OVER GOLD SUPPORTED ON MgO: THE ROLE OF F-CENTERS IN CATALYSIS*

Results

Au/MgO catalysts were prepared by an impregnation method using the tetranuclear amidinate gold(I) complex $[Au_4(form)_4]$, form = [(*p*-tolyl)NCN(*p*-tolyl)] [85], as described in Chapter II. Magnesium oxide was annealed to various temperatures between 900 and 1300 K for 13 hours prior to deposition of the Au complex. Treating MgO at temperatures within this range can produce F-centers within the surface region [53]. Previous work [110, 111] has shown that certain types of F-centers in MgO are stable below 1100 K, and therefore the process of depositing Au and the subsequent pretreatment should not alter the relevant defect concentration at the MgO surface. To understand the role of F-centers in the activation of gold catalysts, the oxidation of CO was studied over these Au/MgO catalysts and the results are given in this chapter.

CO oxidation was carried out from room temperature to 573 K on the Au/MgO catalysts where the MgO support was annealed to various temperatures prior to deposition of the Au. The conversion of CO as a function of reaction temperature is shown in Fig. 10. There is a general trend in the figure that the CO conversion at a given reaction temperature increases with increasing MgO annealing temperature. This is

*Reproduced with permission from "The Role of F-Centers in Catalysis by Au Supported on MgO", Z. Yan, S. Chinta, A. A. Mohamed, John P. Fackler, Jr., and D. Wayne Goodman, *Journal of the American Chemical Society*, 2005, 127, 1604-1605. Copyright [2005] American Chemical Society.

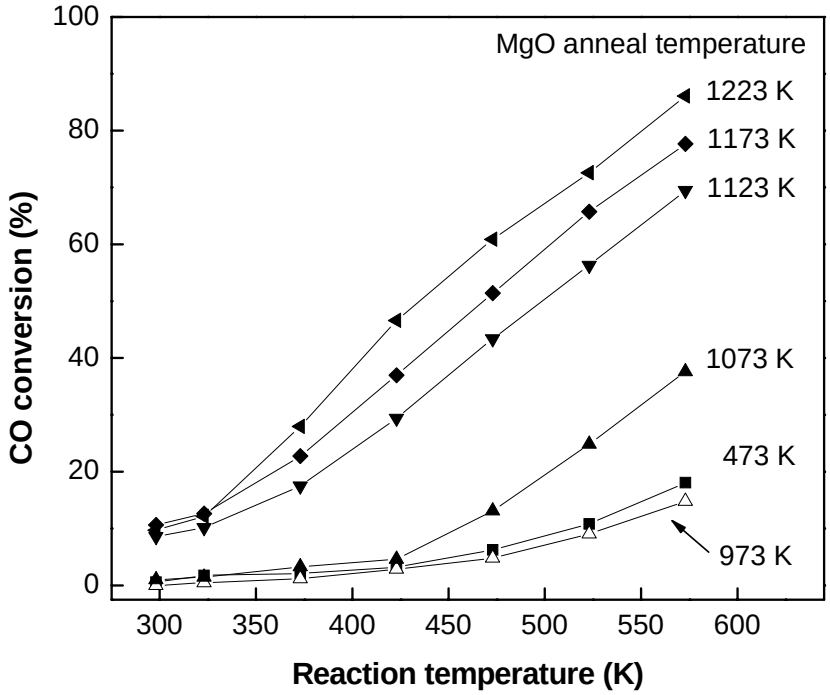

Fig. 10. CO conversion as a function of reaction temperature on Au/MgO catalysts, where MgO support was annealed to the indicated temperature prior to deposition of the Au.

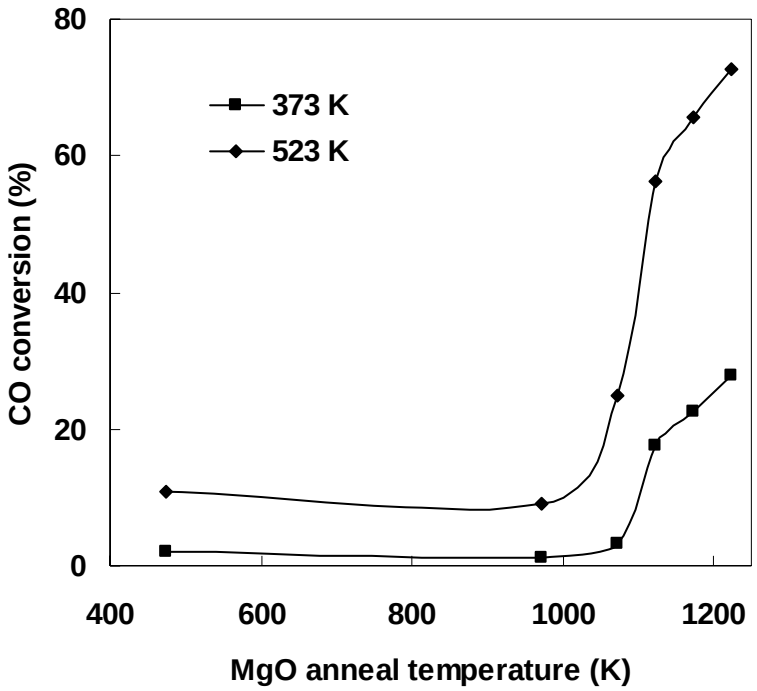

Fig. 11. The CO conversions at 373 K and 523 K as a function of the MgO anneal temperature.

more evident from Fig. 11, which shows the CO conversions at 373 K and 523 K as a function of the MgO annealing temperature. Apparently the activity of Au/MgO increased significantly after the MgO support was annealed to higher than 1123 K prior to deposition of the Au.

Fig. 12 shows the transmission electron micrographs (TEM) of two Au/MgO catalysts, where the MgO support was annealed to 1073 and 1173 K, respectively. The average Au cluster size was 4.3 nm on the 1073 K annealed MgO support and 3.8 nm on the 1173 K annealed sample.

At even higher anneal temperatures (> 1223 K), the surface area of MgO started to decrease dramatically. The BET specific surface area of MgO dropped from 26 to 2 m^2/g as the annealing temperature increased from 1073 to 1273 K. The decrease in surface area resulted in an increase in the Au cluster sizes and a reduction in the CO catalytic oxidation activity, as shown in Fig. 13. The CO conversions on this Au/MgO (MgO was annealed to 1273 K) were significantly lower than those annealed to 1173 or 1123 K.

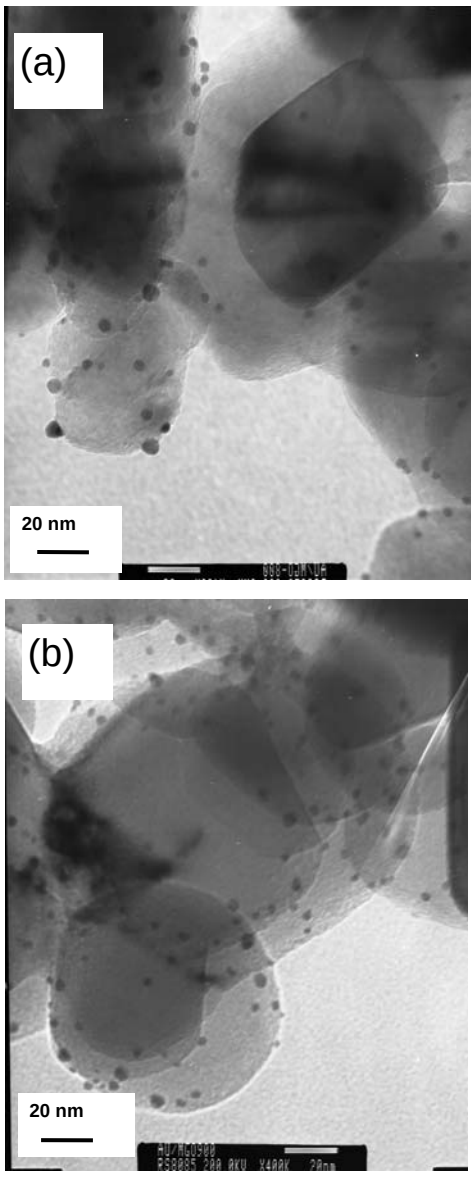

Fig. 12. (a) Transmission electron micrograph of a Au/MgO catalyst where the MgO support was annealed to 1073 K prior to deposition of the Au. (b) Transmission electron micrograph of a Au/MgO catalyst where the MgO support was annealed to 1173 K prior to deposition of the Au.

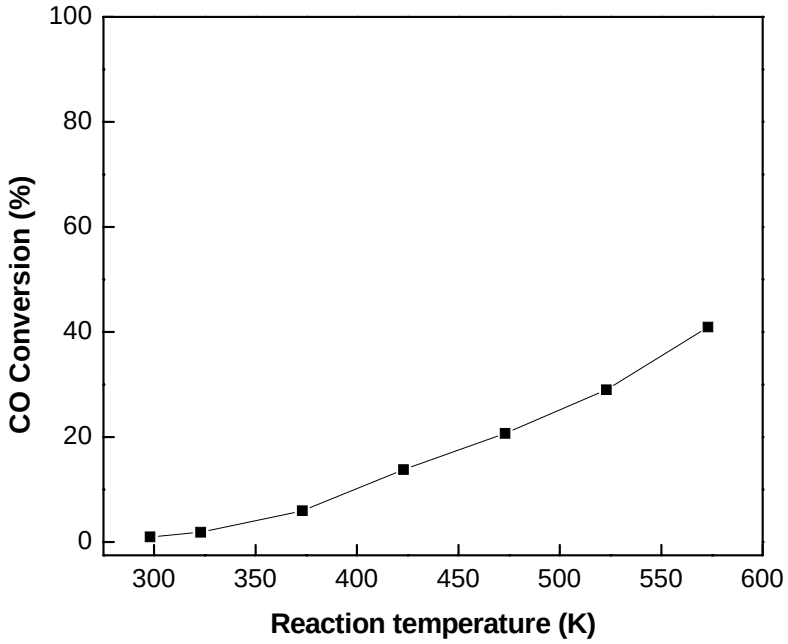

Fig. 13. CO conversion as a function of reaction temperature on a Au/MgO catalyst where the MgO support was annealed to 1273 K prior to deposition of the Au.

Discussion

Previous studies have shown that thermal treatment of MgO to high temperature can produce F-centers within the surface region and the concentration of F-centers is proportional to the annealing temperature [53, 110-113]. Wu et al. studied the electronic transitions associated with various defects in MgO films on Mo(100) using electron loss spectroscopy (EELS) [53]. They found that defects in MgO can be generated at temperatures higher than 1100 K. Specific defect assignments were determined by direct comparison with data acquired for bulk MgO. A loss feature at 5.33 eV was assigned to surface F-centers (oxygen vacancies containing two electrons). In Fig. 14b, the normalized intensity of the EELS feature identified as due to F-centers in or near the MgO surface is plotted against the annealing temperature of the MgO film [53]. For comparison, our data of CO oxidation on supported Au/MgO catalysts are shown in Fig. 14a, where the CO conversion at 373 K is plotted against the annealing temperature of the MgO support. The results in Fig. 14 show a direct correlation between the change in the catalytic activity of the subsequently deposited Au clusters and the change in the concentration of F-centers in the MgO support. This correlation suggests that F-centers play a direct role in the activation of the Au clusters.

The similar role of F-centers in the oxidation of CO by Au has also been observed experimentally on MgO films by Landman and coworkers [51, 114]. They studied the oxidation of CO on size-selected gold clusters using temperature-programmed reaction (TPR) experiments, and found that the catalytic activity increased dramatically when gold clusters were deposited on defect-rich MgO(110) films [51].

Theoretical calculations have shown that the role of F-centers is twofold. First, the adsorption energy of Au atoms on F-centers is larger than that on a perfect oxide surface, thus preventing Au atoms from forming larger particles [51, 115]. For example, the binding energy of Au_8 clusters on a defect-rich MgO surface is about 2.2 eV higher than that on a defect-free MgO surface [51]. Similarly, on the rutile TiO_2(110) surface, the adsorption energy of a single Au atom on an oxygen vacancy site is more stable by 0.45 eV than on the stoichiometric surface [50]. Our TEM results showed that the Au clusters on the 1073 K annealed MgO support were larger than those on the 1173 K annealed sample, which is consistent with an enhanced stability of Au clusters bound to a defect-rich MgO surface.

Secondly, F-centers on oxide surfaces can activate Au by partial electron transfer from the oxide surface to gold particles, thus promoting their catalytic activity [7, 9]. For example, the charge transfer from oxide to gold is 0.5 e for MgO [51] and 0.15 e for TiO_2 [115]. These charge transfers enhance the adsorption of oxygen, making gold more active for CO oxidation.

The results for the Au/MgO system are likely relevant to other oxide-supported Au systems, such as Au/TiO_2. A recent model study of Au on a highly reduced TiO_x ordered film grown on Mo(112) has demonstrated that a highly reduced TiO_x support leads to strong bonding between Au and the reduced Ti atoms of the TiO_x support, yielding electron-rich Au [116]. These studies are entirely consistent with recent theoretical studies on the Au/TiO_2 system [115, 117, 118] that show the importance of

reduced Ti defect sites at the boundary between Au clusters and a TiO_2 interface in determining the Au cluster shape and electronic properties.

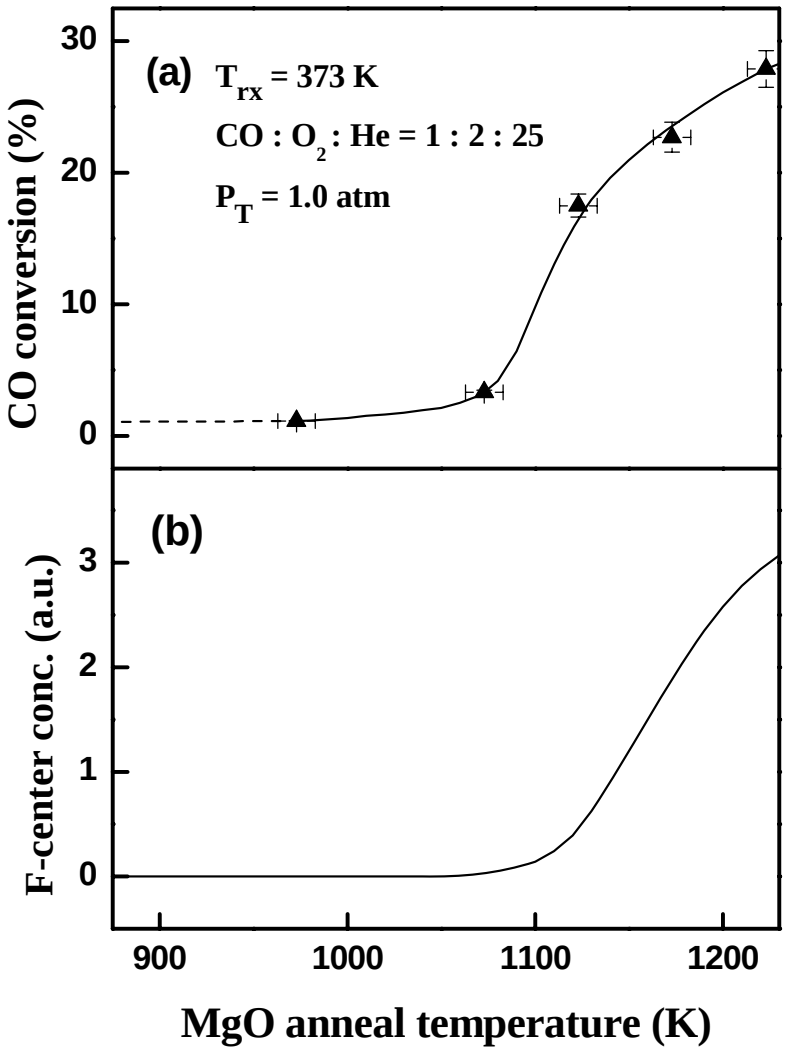

Fig. 14. (a) The conversion of CO to CO_2 by Au/MgO as a function of the anneal temperature of the MgO support prior to deposition of the Au. The data were measured at 373 K in a mixture of CO: O_2: He (1:2:25) maintaining a flow rate of 45 mL/min. (b) The relative concentration of F-centers in MgO as determined by electron energy loss spectroscopy as a function of the anneal temperature [53].

CHAPTER V

CO OXIDATION ON PLATINUM GROUP METALS*

Introduction

Recently in our laboratory, a sharp increase in reaction rate was observed during CO oxidation on platinum group metals at a critical O_2/CO ratio in excess of stoichiometry. When this increase happens, the CO_2 formation rate increases one or two orders of magnitude compared to the rate obtained at a slightly lower O_2/CO ratio. A typical experiment is shown in Fig. 15, where the total pressure of CO and O_2 in a batch reactor is plotted as a function of reaction time. A significant feature in this figure is a sudden pressure drop observed at the 21st minute, indicating the formation of a hyperactive state on the catalyst surface. Numerous investigations, including in situ infrared and XPS characterizations, as well as kinetic studies, have been performed in our laboratory in order to understand the nature and properties of this hyperactive state. In this chapter, the results of the kinetic study of CO oxidation over various forms of Pt-group catalysts, including single crystals, polycrystalline metals, and supported catalysts, will be presented. The critical results from the spectroscopic studies will also be discussed.

*Parts of this chapter have been reprinted from *Surface Science*, M.S. Chen, Y. Cai, Z. Yan, K.K. Gath, S. Axnanda, and D. Wayne Goodman, Highly active surfaces for CO oxidation on Rh, Pd, and Pt, in press, Copyright (2007), with permission from Elsevier.

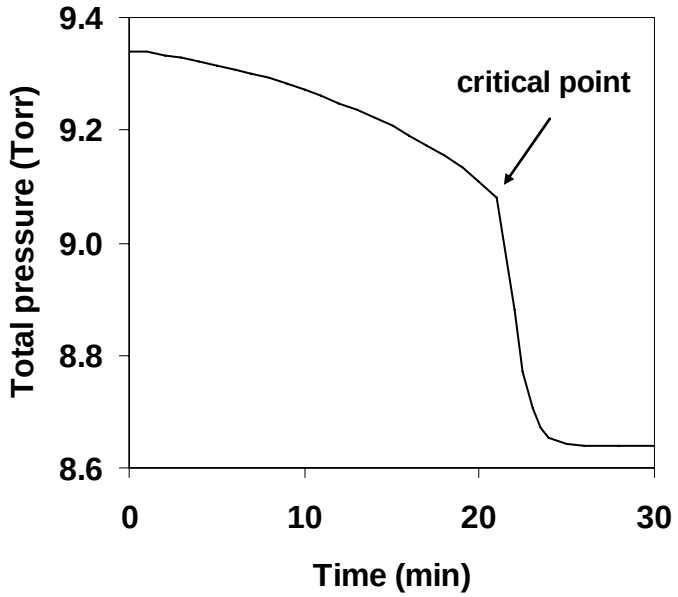

Fig. 15. Total pressure of CO and O_2 as a function of reaction time during a typical experiment of CO oxidation on a Pd catalyst. A critical point is shown at the 21st minute, indicating the formation of a hyperactive state.

CO Oxidation on Single Crystals

Pd(100)

The catalytic oxidation of CO on single crystal surfaces of Pd has been studied extensively at low pressures (< 10^{-6} Torr) [61, 63]. Under these conditions, the surface is almost entirely covered by CO, and the reaction rate is determined by the desorption rate of CO. At elevated pressures (> 1 Torr) and near stoichiometric conditions (O_2/CO = 0.5), the surface is also mainly covered by CO, and the reaction kinetics is almost identical to that at low pressures [63]. However, under strong oxidizing conditions, it is possible to form surface oxides on Pd surfaces [119-121]. Few studies have been performed under such conditions, although these are probably the working conditions of industrial catalysts.

In this section, the results of CO oxidation on a Pd(100) single crystal catalyst under oxidizing conditions will be discussed. The oxidation of CO was performed in a batch reactor using a CO/O_2 gas mixture and the reaction rate was measured by monitoring the change of total pressure. If initial O_2/CO ratios are higher than stoichiometry (O_2/CO > 0.5), the O_2/CO ratio will increase during the reaction until all CO is consumed. This character enabled us to study the reaction rate of CO oxidation continuously as a function of O_2/CO ratio in a batch reactor.

CO oxidation was carried out on a Pd(100) single crystal at 525 K with an initial O_2/CO ratio of 5. Fig. 16 shows the total pressure of CO and O_2 as a function of reaction time. A dramatic pressure drop was observed at the 9^{th} minute in the figure, indicating a sharp increase in reaction rate. At the same time, a jump of the sample temperature was

also noticed due to the sudden release of a large amount of heat from this exothermic reaction. The changes of CO_2 formation rate (number of CO_2 molecules produced per metal atom site per second, or TOF) and CO/O_2 ratio during the reaction are shown in Fig. 17 and Fig. 18. Before the sharp pressure drop, the reaction rate increased slowly with increasing O_2/CO ratio, which was consistent with a negative first-order dependence in CO partial pressure [122, 123]. When the O_2/CO ratio reached a critical value (~10), the reaction rate increased dramatically. The measured maximum TOF in this experiment was about 700, two orders of magnitude higher than the rate (TOF = 5.5) measured at stoichiometric reaction conditions and similar pressures [63]. Experiments performed at various total pressures (5–60 Torr) showed the same phenomenon: there was a sharp increase in the reaction rate at an O_2/CO ratio of ~10 for reactions at 525 K. These results indicate that a hyperactive state formed at a critical O_2/CO ratio. The rate observed subsequent to the rate maximum is somewhat ambiguous because of temperature instabilities due to excessive heat released. However, a linear decrease to zero is anticipated at extremely low CO pressures and predicted from the previous reports [61, 122].

The oxidation of CO was also studied using gas mixtures with various initial O_2/CO ratios. The time required to achieve the hyperactive state increased with a decrease in the initial O_2/CO ratio. However, the critical O_2/CO ratio is practically a fixed value at a given reaction temperature. This implies that the O_2/CO ratio, which defines the chemical potential [124], is the key parameter for the formation of the hyperactive state.

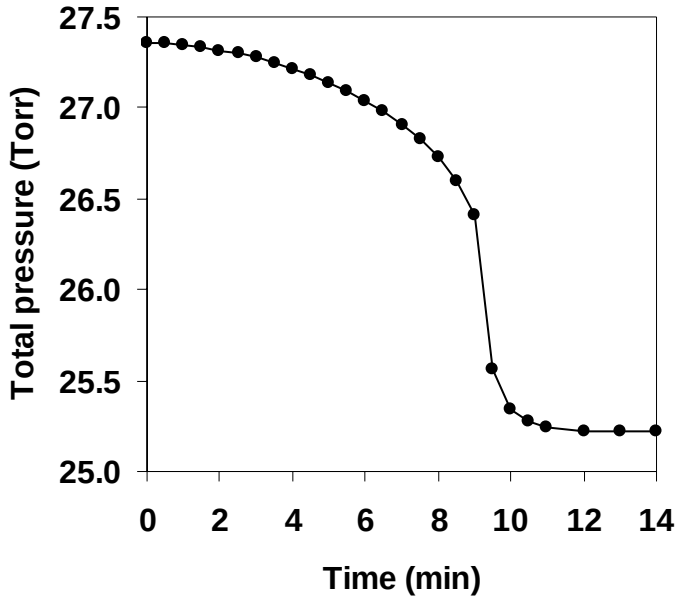

Fig. 16. Total pressure as a function of reaction time for CO oxidation on Pd(100) at 525 K. The reaction was performed with an initial O_2/CO ratio of 5 and a total pressure of 27 Torr.

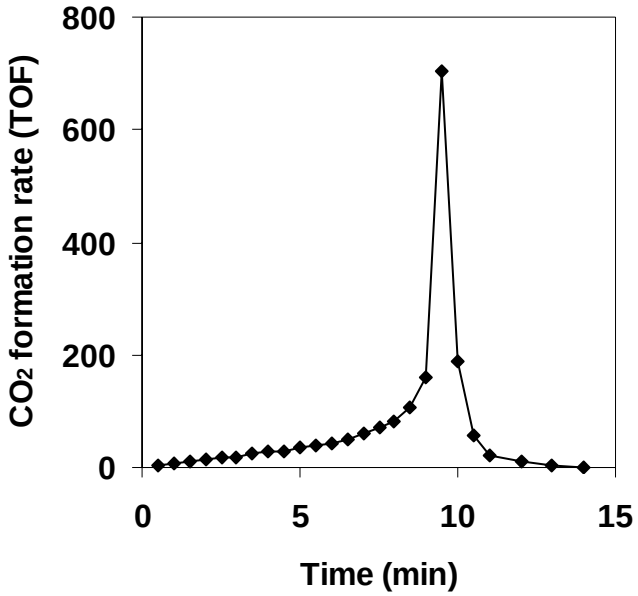

Fig. 17. CO_2 formation rate at 525 K as a function of reaction time for CO oxidation on Pd(100). The reaction was performed with an initial O_2/CO ratio of 5 and a total pressure of 27 Torr.

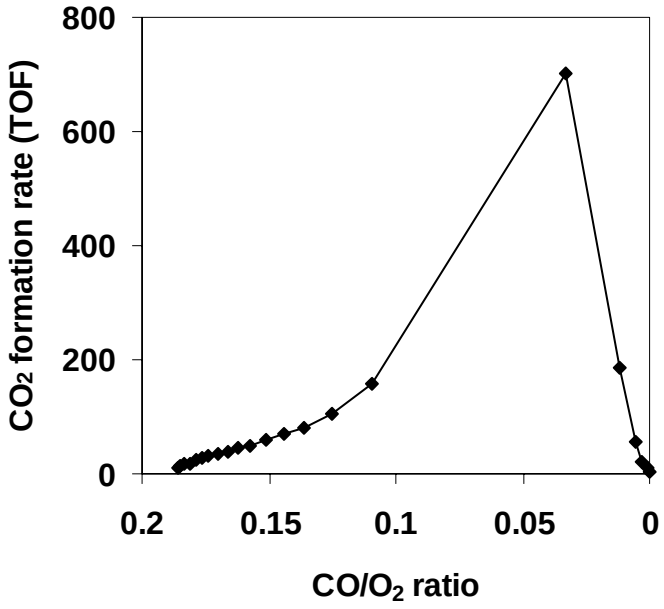

Fig. 18. CO_2 formation rate at 525 K as a function of CO/O_2 ratio for CO oxidation on Pd(100). The reaction was performed with an initial O_2/CO ratio of 5 and a total pressure of 27 Torr.

The fact that the sharp increase in the reaction rate was observed at high O_2/CO ratios suggests the oxygen-covered surface is far more active than a CO-covered surface in a stoichiometric mixture of O_2/CO. Spectroscopic studies [125] were performed in our laboratory in order to understand the nature of this hyperactive surface. In situ PM-IRAS spectra (polarization modulation infrared reflection absorption spectroscopy) showed an intense ν_{CO} feature before the sharp pressure drop, and this feature corresponds to CO bound to metallic Pd. However, the spectra acquired after the dramatic pressure drop showed no adsorbed CO [125], consistent with an oxygen-covered surface. After quenching to room temperature, XPS data showed that after the reaction ~1 ML oxygen was present on the surface. Furthermore, only a very thin oxygen-covered surface (< 2 ML) was formed in pure oxygen at the same oxygen partial pressure. These spectroscopic results confirmed that the hyperactive state is an oxygen-covered surface.

Formation of surface oxides on Pt-group metals has been reported in numerous studies [119-121, 126-132]. For example, Voogt et al. reported the formation of a surface oxide on Pd(111) and on a polycrystalline Pd foil at elevated temperatures (> 470 K) and O_2 pressures (> 10^{-6} Torr) [130]. No diffusion of oxygen to the bulk or to the subsurface layers was observed under their conditions. A ($\sqrt{5}\times\sqrt{5}$)R27° surface structure [132] was observed on Pd(100) with low-energy electron diffraction (LEED) at oxygen coverage lower than that for bulk PdO formation. Density functional theory (DFT) calculations showed that this surface oxide is stable under realistic reaction conditions for CO oxidation [133].

The significantly higher CO oxidation rate observed for an oxygen-rich Pd surface compared to an oxygen-deficient Pd surface is similar to the results observed for Ru, where the CO oxidation rate on a one monolayer oxygen-covered surface is 2 to 3 orders higher than that on a chemisorbed CO-dominant surface [67]. The lower rate on a metallic Pd surface, under conditions close to stoichiometry, is due to the high surface coverage of strongly chemisorbed CO, i.e. the rate is limited by the adsorption/dissociation of O_2 on the surface essentially saturated by CO. In fact, it has been reported that O_2 dissociative adsorption is blocked on a CO-saturated surface [134-136].

In contrast, in a high O_2/CO ratio reactant mixture at elevated pressures, the surface is predominately covered with chemisorbed atomic oxygen, which reacts with neighboring weakly adsorbed CO to form CO_2 [137]. Indeed, this chemisorbed surface oxygen can react with CO at room temperature [138]. The CO_2 formation rate on an oxygen-covered surface will depend on the CO pressure, particularly at UHV conditions, because of the relatively weak adsorption of CO on this surface [61, 139-141]. This explains why the sharp increase in the reaction rate as a function of the O_2/CO ratio at elevated pressures in the present work has not been observed under UHV conditions [61, 139, 140]. In fact, an Eley-Rideal (E-R) reaction pathway between gas phase CO and adsorbed atomic oxygen has been proposed for CO reacting with an oxygen-covered surface [137, 139, 140].

Ru(0001)

As described in Chapter I, the kinetic behaviors of CO oxidation on Ru surfaces are significantly different from those on other Pt group metals [18, 26, 27]. The high activity of Ru catalysts at elevated pressures was attributed to the presence of a monolayer of oxygen on the Ru surface [67]. As a comparison with Pd(100), the oxidation of CO on the Ru(0001) surface was studied under similar conditions, and the results are given in this section.

Fig. 19 and Fig. 20 show the changes of total pressure and CO_2 formation rate as a function of reaction time for CO oxidation on Ru(0001) at 525 K. A different trend was noticed compared to that on Pd(100). As shown in Fig. 19, no sharp pressure drop was observed during the reaction on Ru(0001), and the CO_2 formation rate decreased with increasing O_2/CO ratio until all CO was consumed. The measured TOFs were consistent with the literature values at similar conditions [67].

It is not surprising that the sharp increase in the reaction rate on Pd(100) was not observed on Ru(0001) under these conditions, because the formation of surface oxide on Ru(0001) occurs at much lower O_2/CO ratios [67]. For example, at 500 K, surface oxygen was detected on Ru(0001) at an O_2/CO ratio as low as 1/16, and saturated when the O_2/CO ratio reached 1/4 [67]. In our experiments, to vary O_2/CO ratios continuously, the initial O_2/CO ratio was higher than stoichiometry and became even higher during the reaction. Under such conditions, CO oxidation occurred exclusively on the oxygen-covered Ru surface. The sharp increase in activity observed on Pd(100) was due to the transformation from metallic surface to oxygen-covered surface; therefore, it was not

observed on Ru(0001). To see the sharp rate increase on Ru surfaces, it is necessary to develop a different experimental setup in which the O_2/CO ratio can be increased from lower than stoichiometry (O_2/CO < 0.5).

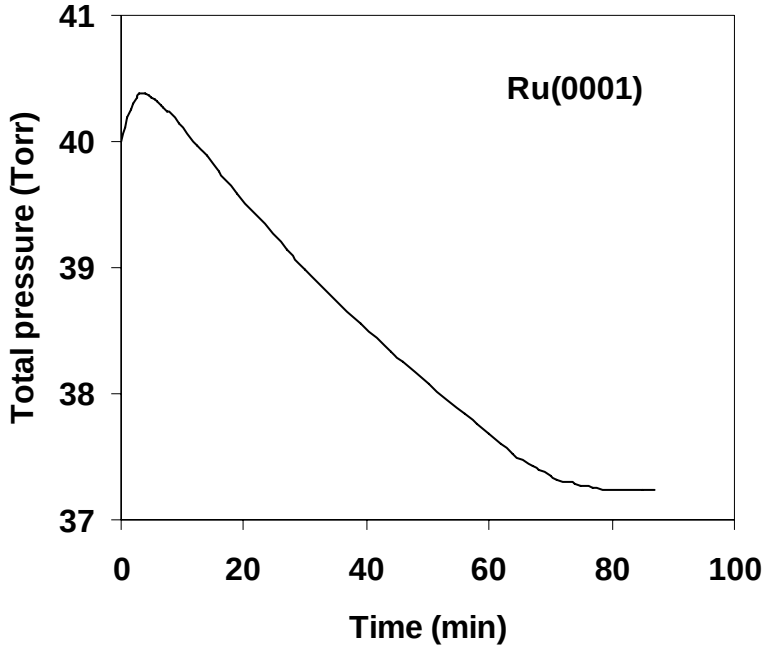

Fig. 19. Total pressure as a function of reaction time for CO oxidation on Ru(0001) at 525 K. The reaction was performed with an initial O_2/CO ratio of 5 and a total pressure of 40 Torr.

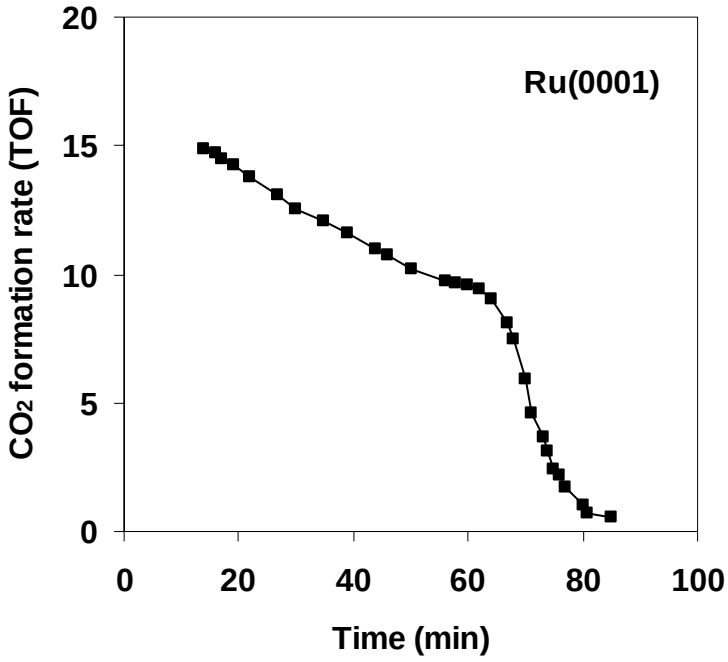

Fig. 20. CO_2 formation rate at 525 K as a function of reaction time for CO oxidation on Ru(0001). The reaction was performed with an initial O_2/CO ratio of 5 and a total pressure of 40 Torr.

CO Oxidation on Polycrystalline Metals

The catalytic oxidation of CO on platinum group metals is generally considered to be structure insensitive, which means that polycrystalline metals should exhibit the same kinetic behaviors as single crystals [63, 66]. Therefore, the reaction kinetics and mechanism on polycrystalline metals can be predicted by those obtained on single crystals, and vice versa. In fact, our results of CO oxidation on polycrystalline Pd wires showed an excellent agreement with those on Pd(100), as shown in this section. Furthermore, to understand the nature of the hyperactive surfaces, the oxidation of CO was also studied on polycrystalline wires of other Pt group metals, including Rh and Pt.

Pd wire

The oxidation of CO was studied using a small polycrystalline Pd wire (4–5 mm long) under similar conditions to those on single crystals. A sharp drop in total pressure during reaction is evident in Fig. 21, similar to what we observed on Pd(100). At the same time, the CO_2 formation rate increased almost 10 times (figure on page 63). The O_2/CO ratio (~10) at the critical point was very close to that obtained on Pd(100). This indicates that the O_2/CO ratio required to achieve the hyperactive state is virtually the same for a given metal and reaction temperature, regardless of the surface structures.

CO oxidation was also performed using gas mixtures with various total pressures or initial O_2/CO ratios. The critical O_2/CO ratio at the sharp pressure drop remained unchanged at a certain reaction temperature. This is again consistent with the results on Pd(100), and implies the key role of oxygen chemical potentials for the formation of the hyperactive state.

Rh and Pt wires

Similar experiments were performed on polycrystalline wires of Rh and Pt (Fig. 21–Fig. 25). The formation of hyperactive states at high O_2/CO ratios, evidenced by the sharp pressure drops and dramatic increases in the reaction rate, were also observed on Rh and Pt, even though a higher temperature and O_2/CO ratio were required for Pt. The CO_2 formation rate as a function of O_2/CO ratio for Rh, Pd, and Pt are compared in Fig. 25. The hyperactive state on Rh, Pd, and Pt formed at O_2/CO ratios of approximately 8.6, 10, and 28, respectively.

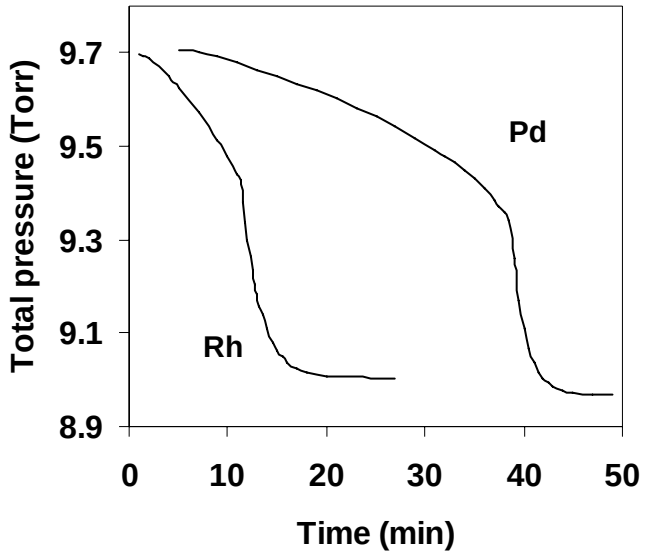

Fig. 21. Total pressure as a function of reaction time for CO oxidation on Pd and Rh wires at 525 K. The reaction was performed with an initial O_2/CO ratio of 5 and a total pressure of 9.6 Torr.

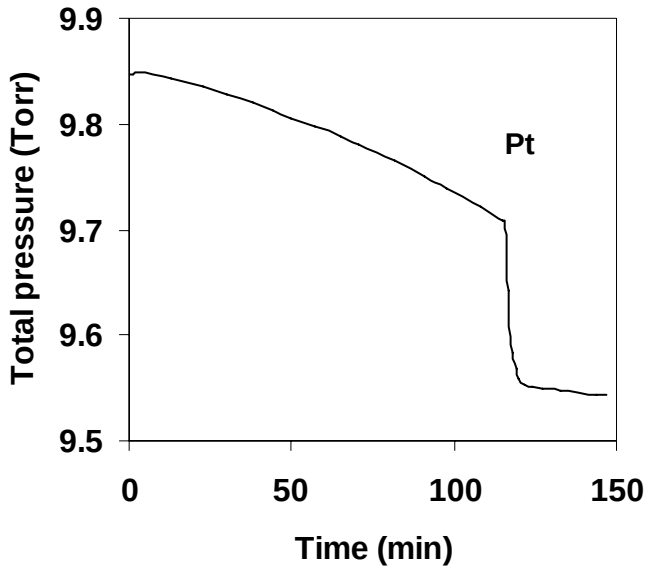

Fig. 22. Total pressure as a function of reaction time for CO oxidation on a Pt wire at 550 K. The reaction was performed with an initial O_2/CO ratio of 15 and a total pressure of 9.6 Torr.

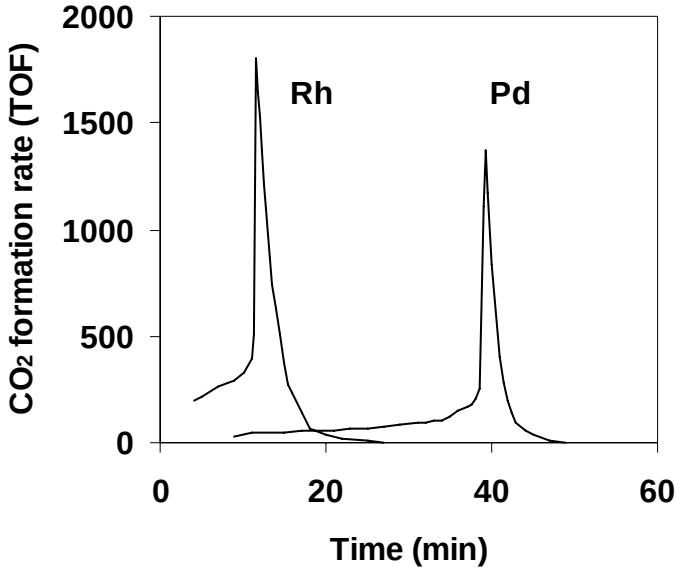

Fig. 23. CO_2 formation rate at 525 K as a function of reaction time for CO oxidation on Pd and Rh wires. The reaction was performed with an initial O_2/CO ratio of 5 and a total pressure of 9.6 Torr.

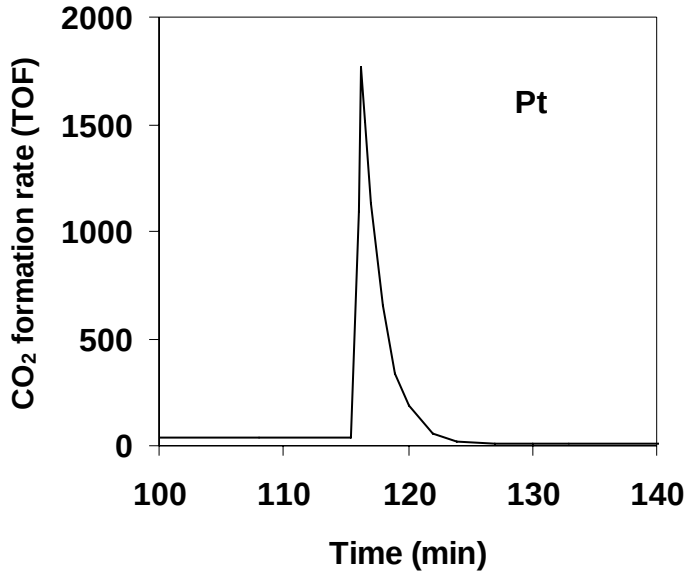

Fig. 24. CO_2 formation rate at 550 K as a function of reaction time for CO oxidation on a Pt wire. The reaction was performed with an initial O_2/CO ratio of 15 and a total pressure of 9.6 Torr.

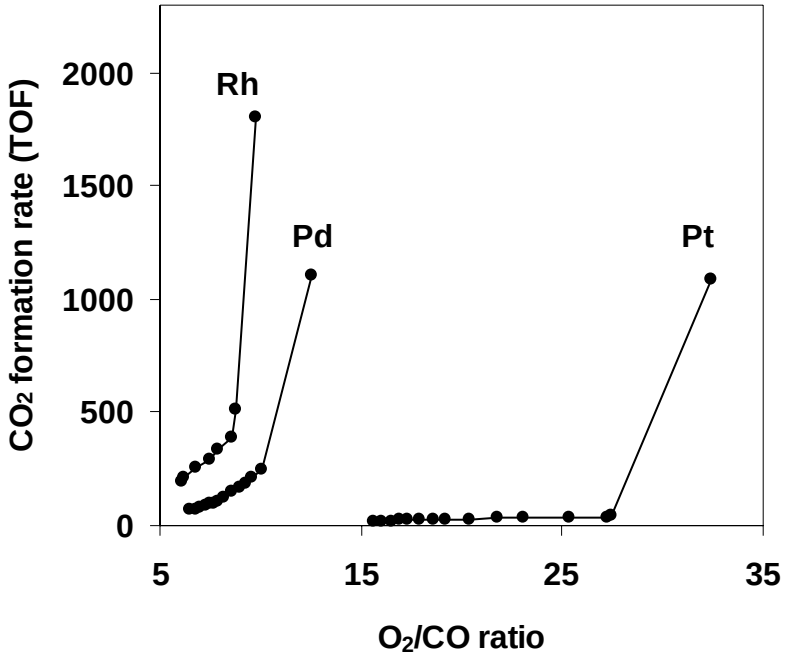

Fig. 25. CO_2 formation rate as a function of O_2/CO ratio for CO oxidation on Rh, Pd, and Pt wires. The reaction temperature was 550 K for Pt and 525 K for Rh and Pd.

As discussed previously, the catalytic hyperactive state corresponds to an oxygen-covered surface; therefore, the adsorption energy of oxygen and the stability of the corresponding metal oxide should play a key role in determining the oxygen chemical potential for achieving the hyperactive state [124]. In addition, the adsorption energies of CO should be important since the active surface changes from predominantly CO to predominantly chemisorbed oxygen. O_2 dissociative adsorption energies of 334, 234, 230, and 188 kJ/mole-oxygen atoms are reported for the close-packed Ru [142], Rh [143], Pd [144], and Pt [145] surfaces, respectively. Whereas, the adsorption energies for CO on these surfaces are very close: 122, 130, 142, and 138 kJ/mole, respectively, for the close-packed Ru, Rh, Pd, and Pt surfaces [146-148]. The order of the O_2/CO ratios required for Pt, Pd, Rh, and Ru to achieve the hyperactive state in Fig. 25 was found to relate directly to the oxygen adsorption energies and also the standard heats of formation for RuO_2, Rh_2O_3, PdO, and PtO of -305, -178, -116, and -71 kJ/mole (per mole metal atoms), respectively [149]. The relatively large oxygen adsorption energy and oxide formation energy for Ru lead to the formation of a highly active, oxygen-covered surface at an O_2/CO ratio even lower than stoichiometry [67]. In contrast, the relatively low adsorption energy of oxygen on Pt precludes the formation of the hyperactive state at 525 K even at O_2/CO ratios as high as 50. Experiments carried out at 550 K on Pt, on the other hand, showed a sharp rate increase at high O_2/CO ratios. The temperature effect on the critical O_2/CO ratios will be discussed in detail in the next section. Regarding the fact that the active surface transforms from a CO-covered to an O-covered surface at high O_2/CO ratios, the difference in surface free energies of these

two is (G(O) – G(CO)) for a given metal surface. These values of free energies can be estimated by the heats of adsorption of oxygen and CO on a given metal surface, i.e. (E_O – E_{CO}). As described by Campbell [124], to overcome this energy barrier at a given

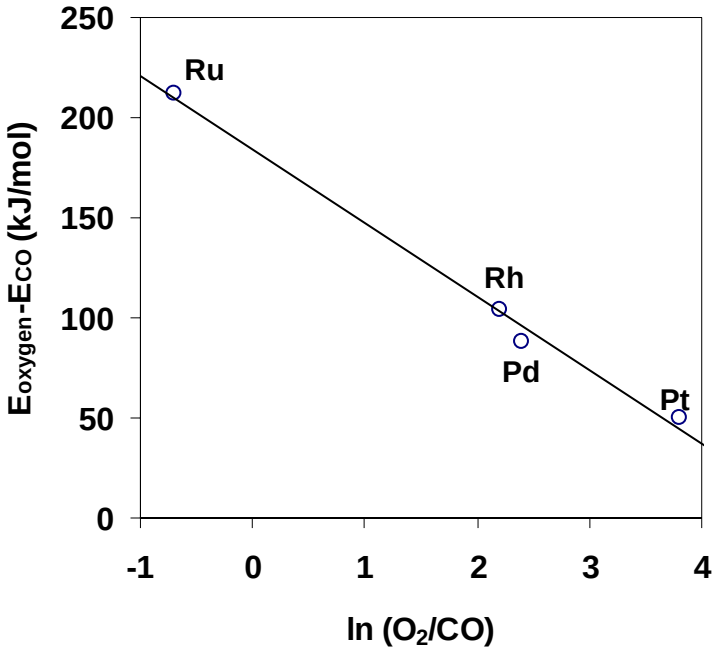

Fig. 26. Differences in O_2 and CO adsorption energies on Ru, Rh, Pd, and Pt versus the logarithm of the critical O_2/CO ratios required to achieve the hyperactive state on that metal at a given temperature.

temperature, this energy should be directly related to $\ln(P_{O2}/P_{CO})$. Indeed, a linear relationship was observed in a plot of the adsorption energy differences for various Pt-group metals versus the logarithm of the critical O_2/CO ratios, as shown in Fig. 26.

Effect of reaction temperature

Based on the discussion above, the critical O_2/CO ratio required to achieve the hyperactive state should be lower if the surface temperature is increased. Our results of CO oxidation at various reaction temperatures have confirmed this prediction.

The experiments were performed on a Pd wire using an initial O_2/CO ratio of 2. The results are shown in Fig. 27–Fig. 29. The critical O_2/CO ratios were 9.6, 5.8, and 3.4 for reaction temperatures of 550, 575, and 600 K, respectively. Fig. 30 plots the logarithms of these O_2/CO ratios versus inverse temperature. The linear relationship is consistent with Campbell's theoretical analysis that $\ln(P_{O2}/P_{CO})$ is related to the adsorption energies of O_2 and CO [124].

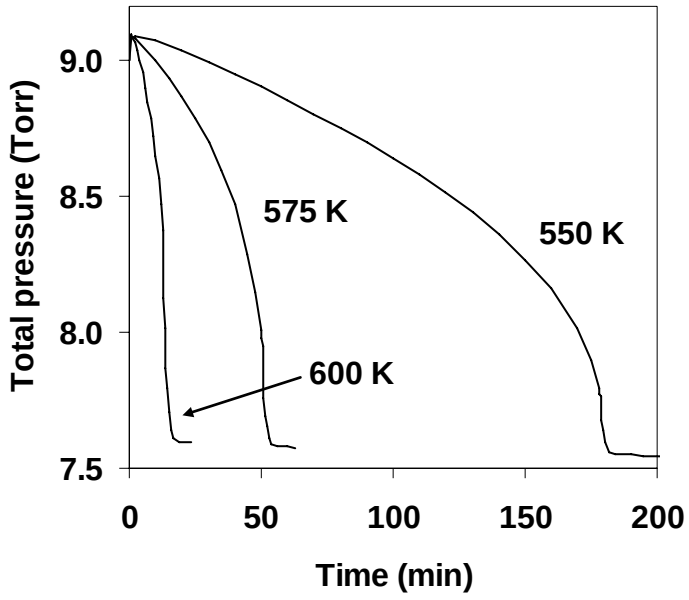

Fig. 27. Total pressure as a function of reaction time for CO oxidation on a Pd wire at 550, 575, and 600 K. The reaction was performed with an initial O_2/CO ratio of 2 and a total pressure of 9 Torr.

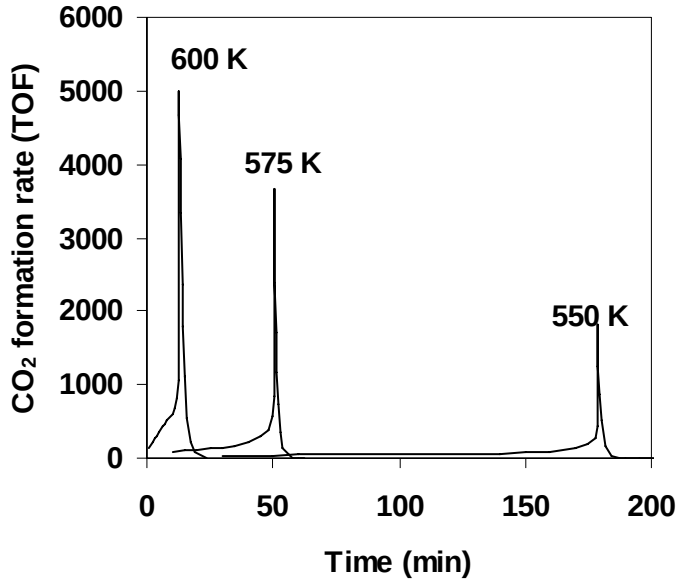

Fig. 28. CO_2 formation rates at 550, 575, and 600 K as a function of reaction time for CO oxidation on a Pd wire. The reaction was performed with an initial O_2/CO ratio of 2 and a total pressure of 9 Torr.

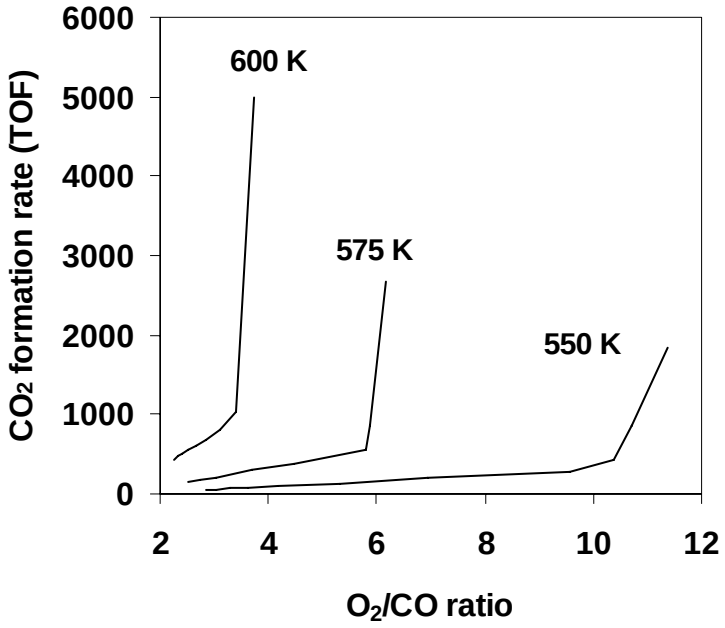

Fig. 29. CO_2 formation rates at 550, 575, and 600 K as a function of O_2/CO ratio for CO oxidation on a Pd wire. The reaction was performed with an initial O_2/CO ratio of 2 and a total pressure of 9 Torr.

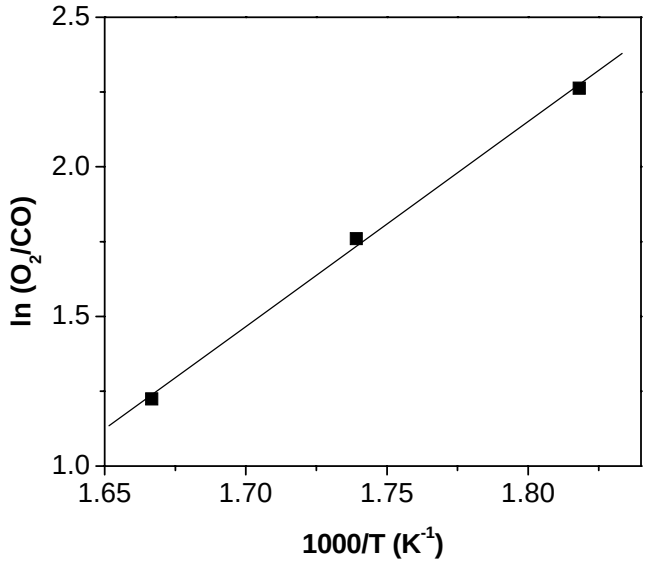

Fig. 30. Logarithm of the critical O_2/CO ratios required to achieve the hyperactive state on Pd as a function of inverse temperature. The reactions were carried out on a Pd wire with an initial O_2/CO ratio of 2 and a total pressure of 9 Torr.

The formation of hyperactive states was also studied under stoichiometric reaction conditions. The oxidation of CO was performed on a Pd wire using a 2:1 CO/O_2 mixture and the reaction temperature was linearly increased. Fig. 31 shows the changes of pressure and reaction temperature as a function of reaction time. As can be seen, the pressure started to drop exponentially at temperatures higher than ~600 K. From the pressure change alone, it was difficult to tell if a hyperactive state formed because the increase in temperature may also cause the sharp pressure drop. However, although the reaction temperature was automatically controlled to increase linearly with time, a sudden temperature jump (Fig. 32) was observed at 655 K, indicating a sharp increase in the reaction rate. The measured TOF at 655 K was about 1.6×10^4, which is much higher than that obtained on Pd(100) at the same temperature under stoichiometric conditions [63]. Apparently, a hyperactive state formed at 655 K under stoichiometric reaction conditions on Pd. The relationship between the O_2/CO ratio (2:1) and the critical temperature (655 K) was consistent with the trend in Fig. 30.

This experiment indicates that surface oxides on Rh, Pd, or Pt can form in stoichiometric or even reducing reaction conditions ($O_2/CO < 0.5$) just as on Ru, provided that the reaction temperature is high enough. On Ru, surface oxides form at lower temperatures at a given O_2/CO ratio, or at lower O_2/CO ratios at a certain temperature compared to those on Rh, Pd, or Pt. Therefore, there are no essential differences between Ru and other Pt group metals.

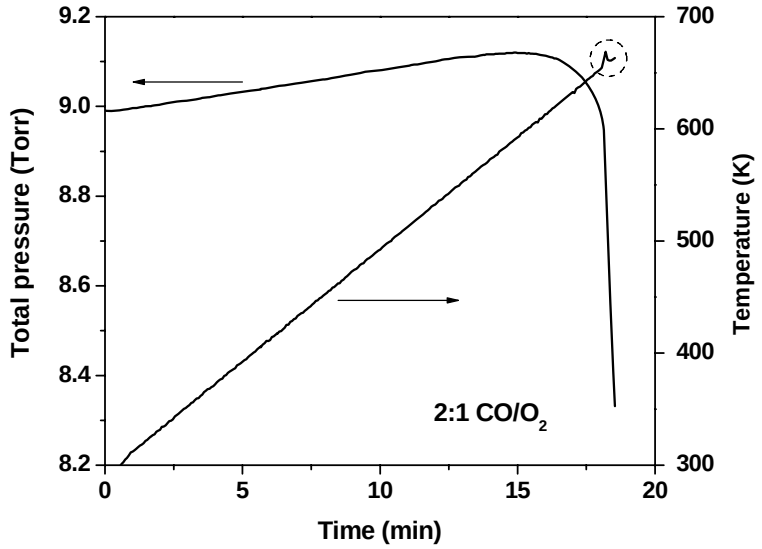

Fig. 31. The changes of total pressure and reaction temperature as a function of time for 2:1 CO/O_2 reaction on a Pd wire. The temperature was increased at 20 K/min.

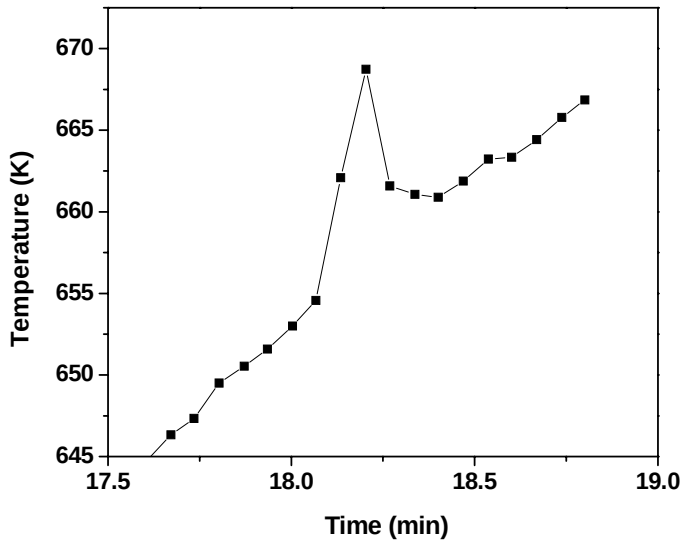

Fig. 32. Reaction temperature as a function of time for CO oxidation on a Pd wire. A temperature jump due to a sudden increase in the reaction rate is shown. The reaction conditions are the same as in Fig. 31.

CO Oxidation on Supported Catalysts

Nanoparticles have attracted increasing research attention during the past decades due to their interesting size-dependent properties [150, 151]. Physicists predicted that the electronic properties of nanoparticles can differ from their bulk materials due to quantum size effects [152].

Metallic nanoparticles often exhibit remarkably different catalytic properties compared to the corresponding infinite surface. It has been found that small particles are easier to oxidize than large particles [153-156]. For example, in a study of the interaction of O_2 with Pd particles (2–10 nm) supported on Al_2O_3(0001), Penner et al. showed that small particles were completely oxidized upon treatment with 25 Torr O_2, whereas most of the larger particles were oxidized to a PdO-like thin film. Schalow et al. [155] observed similar results for the oxidation of Pd nanoparticles supported on Fe_3O_4. They found that small Pd particles (< 3 nm) were fully oxidized with moderate O_2 exposures, but larger particles (4–10 nm) were only partially oxidized. These studies suggest that the formation of surface oxides should occur at a lower oxygen chemical potential for nanoparticles than for single crystals or polycrystalline metals. In fact, as shown in this section, our study of CO oxidation on supported Pd/Al_2O_3 catalysts has confirmed this prediction.

Pd/Al_2O_3(NM)

The oxidation of CO was studied over three 7% Pd/Al_2O_3 catalysts provided by Professor A. K. Datye at the University of New Mexico. These samples are denoted as

Pd/Al_2O_3(NM), and the average Pd particle sizes were 7, 13, and 35 nm, respectively. Compared to the reaction temperature used for single crystals and polycrystalline wires, a much lower temperature (450 K) was used for these powdered samples due to their extremely high activities. Despite this difference in the reaction temperature, the same behavior was observed, as shown in Fig. 33 and Fig. 34. At a critical O_2/CO ratio, a sharp increase in the reaction rate occurred, as evidenced by the sharp drop of pressure.

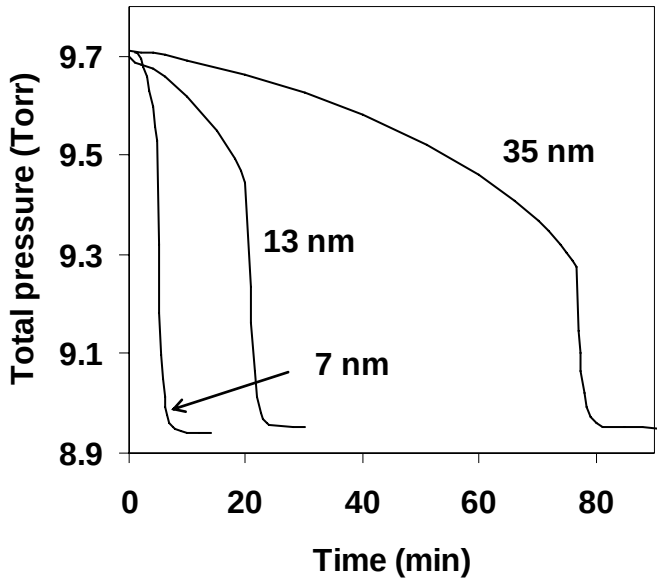

Fig. 33. Total pressure as a function of reaction time for CO oxidation over three 7% Pd/Al_2O_3(NM) catalysts at 450 K. The average Pd particle sizes were 7, 13, and 35 nm, respectively. The data were measured using 1 mg of Pd/Al_2O_3 with an initial O_2/CO ratio of 5 and a total pressure of 9.6 Torr.

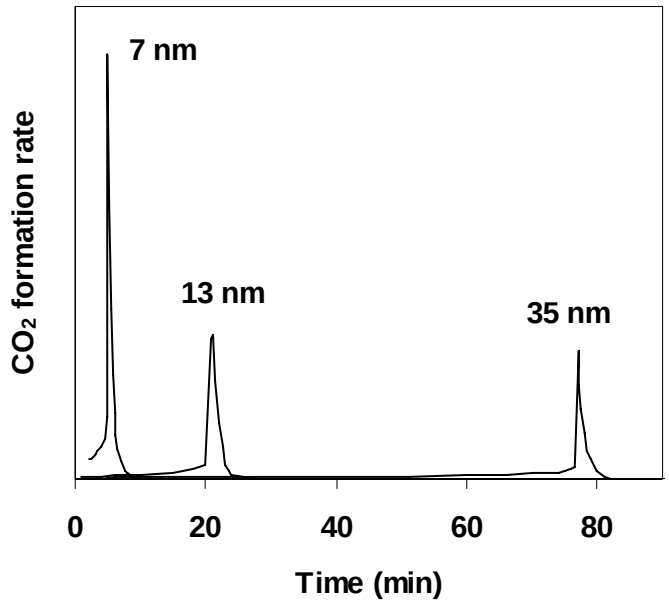

Fig. 34. CO_2 formation rate as a function of time for CO oxidation over three 7% Pd/Al_2O_3(NM) catalysts at 450 K. The average Pd particle sizes were 7, 13, and 35 nm, respectively. The data were measured using 1 mg of Pd/Al_2O_3 with an initial O_2/CO ratio of 5 and a total pressure of 9.6 Torr.

The critical O_2/CO ratios at the sharp pressure drop were 6.4, 8.0, and 12 for particle sizes of 7, 13, and 35 nm, respectively (Fig. 35). The same order for the O_2/CO ratios and the particle sizes implies that a hyperactive oxygen-covered surface formed at a lower oxygen chemical potential for smaller Pd particles than for larger particles. These results are consistent with the previous discussion that small particles are easier to oxidize than large particles.

The variation of critical O_2/CO ratios with particle sizes proved that the sharp increase in the reaction rate was not caused by partial pressure changes of reactant gases (CO or O_2). The negative first-order dependence in CO partial pressure may cause the reaction rate to increase with time at high O_2/CO ratios. However, this increase should be continuous and would not show any break point at a certain O_2/CO ratio. More importantly, if the sharp increase was caused by decreasing CO partial pressure, the critical O_2/CO ratio would not depend on Pd particle sizes. Therefore, the particle size dependence provided additional evidence for the formation of a hyperactive state.

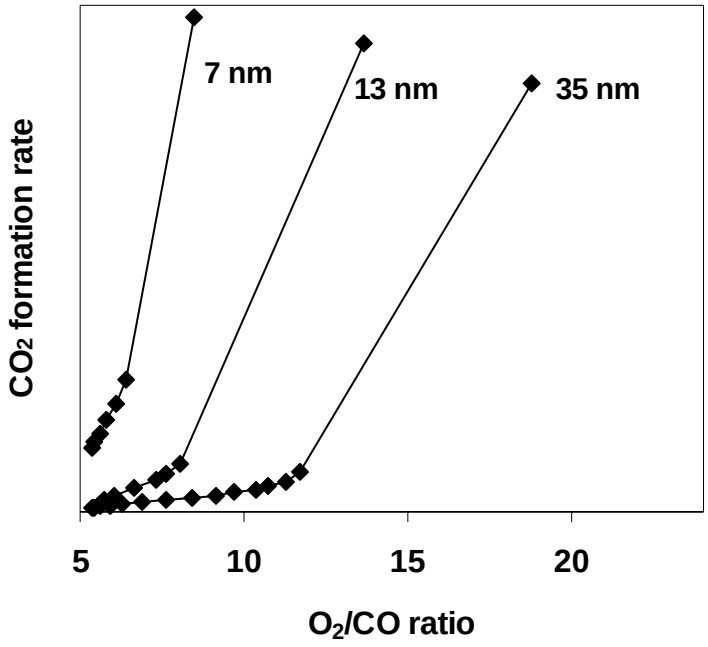

Fig. 35. CO_2 formation rate as a function of O_2/CO ratio for CO oxidation over three 7% Pd/Al_2O_3(NM) catalysts at 450 K. The average Pd particle size is 7, 13, and 35 nm, respectively. The data were measured using 1 mg of Pd/Al_2O_3 with an initial O_2/CO ratio of 5 and a total pressure of 9.6 Torr.

$Pd/Al_2O_3(TW)$

For comparison, other Pd/Al_2O_3 catalysts were studied for the oxidation of CO. These Pd/Al_2O_3 samples were provided by Dr. Chen-Bin Wang at National Defense University, Taiwan [89], and were denoted as Pd/Al_2O_3(TW).

The results of CO oxidation on a 10% Pd/Al_2O_3(TW) catalyst are shown in Fig. 36–Fig. 38. The CO_2 formation rate increased smoothly as the reaction proceeded, and the maximum rate was comparable to those obtained on the Pd/Al_2O_3(NM) samples. However, no sharp increase in the reaction rate was observed. This is significantly different from what we have seen previously on Pd(100), Pd wires, and Pd/Al_2O_3(NM) samples.

The fact that this Pd/Al_2O_3(TW) catalyst became very active at high O_2/CO ratios suggests the formation of hyperactive states. However, the absence of a critical O_2/CO ratio implies that this sample had a wide distribution of particle sizes. Pd particles of various sizes were oxidized to form surface oxides continuously at different O_2/CO ratios; therefore, no critical O_2/CO ratio was observed. This indicates that, in order to exhibit the same phenomenon as on single crystals or polycrystalline metals, supported catalysts must have a very narrow particle size distribution.

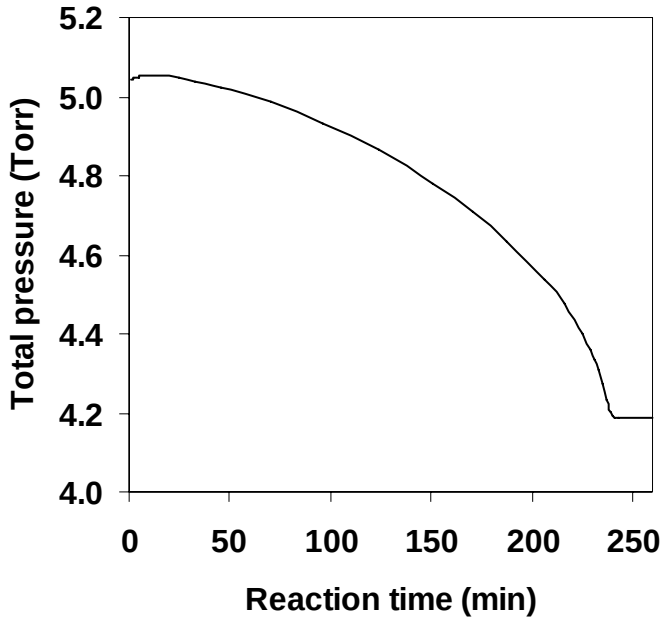

Fig. 36. Total pressure as a function of reaction time for CO oxidation on a 10% Pd/Al_2O_3(TW) catalyst at 450 K. The data were measured using 1 mg of Pd/Al_2O_3 with an initial O_2/CO ratio of 2 and a total pressure of 5 Torr.

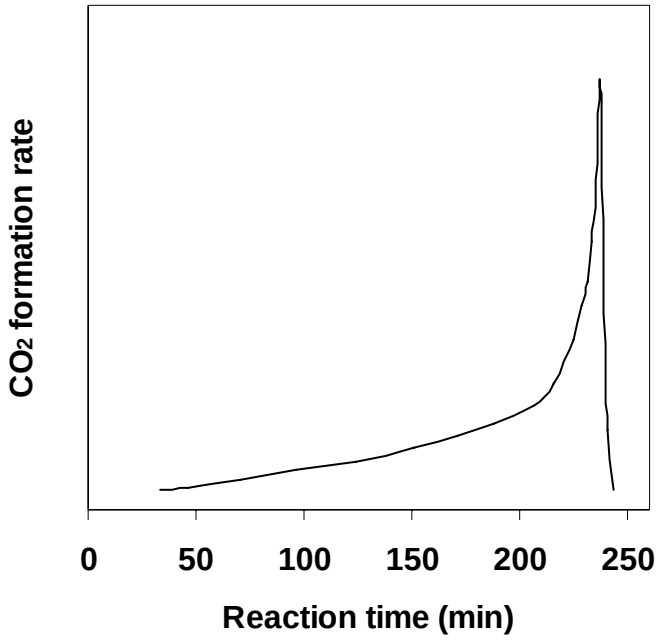

Fig. 37. CO_2 formation rate at 450 K as a function of reaction time for CO oxidation on a 10% Pd/Al_2O_3(TW) catalyst. The data were measured using 1 mg of Pd/Al_2O_3 with an initial O_2/CO ratio of 2 and a total pressure of 5 Torr.

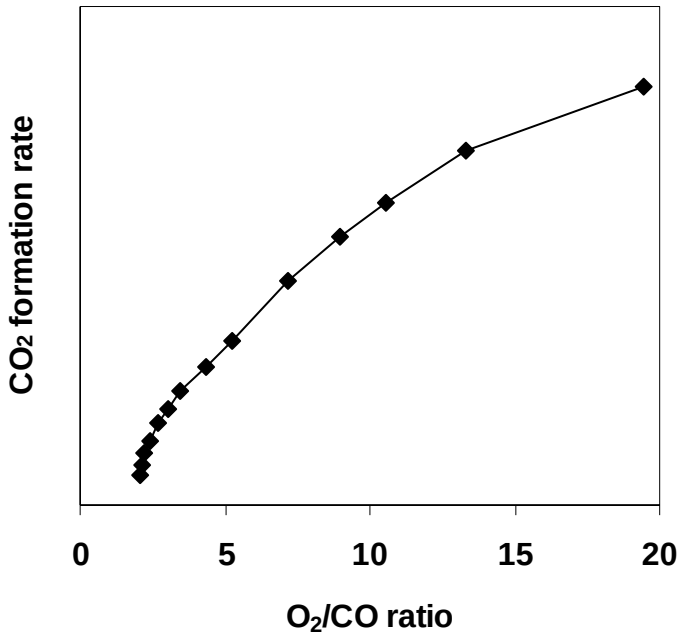

Fig. 38. CO_2 formation rate as a function of O_2/CO ratio for CO oxidation on a 10% Pd/Al_2O_3(TW) catalyst at 450 K. The data were measured using 1 mg of Pd/Al_2O_3 with an initial O_2/CO ratio of 2 and a total pressure of 5 Torr.

Au/TiO_2

Gold nanoparticles supported on metal oxides are highly active for CO oxidation at low temperatures, as discussed in Chapters I and III. Although this system has been studied extensively over the last two decades, the nature of active sites and reaction mechanisms are still under debate. Some studies suggested that cationic gold was more active than zerovalent gold for CO oxidation [157-160]. This may relate to our results on Pt-group metals that oxygen-covered surfaces were more active than clean surfaces. The results of CO oxidation on Au/TiO_2 are given in this section, and are compared with those on Pd/Al_2O_3.

An Au/TiO_2 reference catalyst supplied by the World Gold Council was used in this study. CO oxidation was carried out at room temperature using 5:1 O_2/CO mixtures. To check the effect of deactivation, the reaction was repeated on the used catalyst at the same conditions. The results are shown in Fig. 39 and Fig. 40. Both experiments (1^{st} run and 2^{nd} run) showed decreasing reaction rates with time. The 2^{nd} run showed slight deactivation of the gold catalyst, and the 3^{rd} run (not shown in the figures) was virtually the same as the 2^{nd} run. This indicates that the continuous decrease in activity with increasing O_2/CO ratios was not caused by catalyst deactivation, but by decreasing CO partial pressures.

Further experiments were carried out using various O_2 partial pressures while keeping the CO partial pressure constant. The data showed a steady reaction rate for O_2/CO ratios up to 250.

These results were different from those on Pd catalysts in that a hyperactive state was not observed on Au/TiO_2. However, this could not rule out the possibility of a hyperactive state on Au. Stronger oxidizing conditions (higher reaction temperature and higher O_2 partial pressure) may be required to form an oxygen-covered surface on gold.

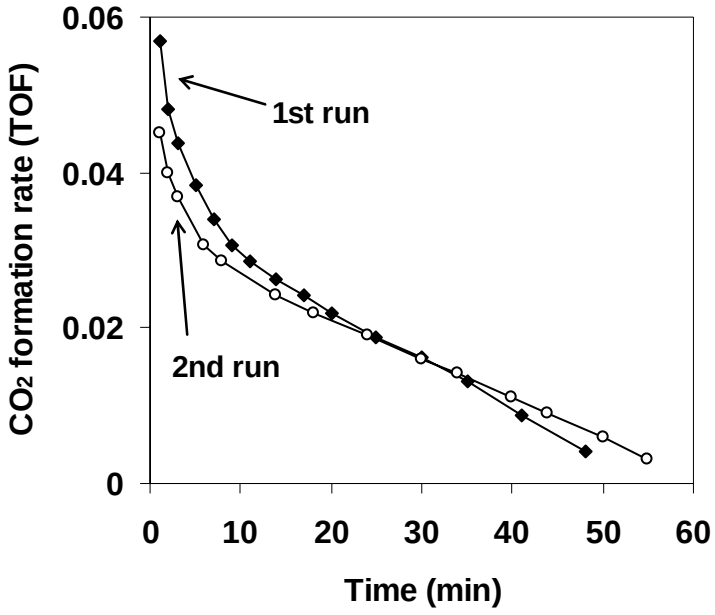

Fig. 39. CO_2 formation rate as a function of reaction time for CO oxidation over an Au/TiO_2 reference catalyst at room temperature. The data were measured using 3 mg of Au/TiO_2 with an initial O_2/CO ratio of 2.

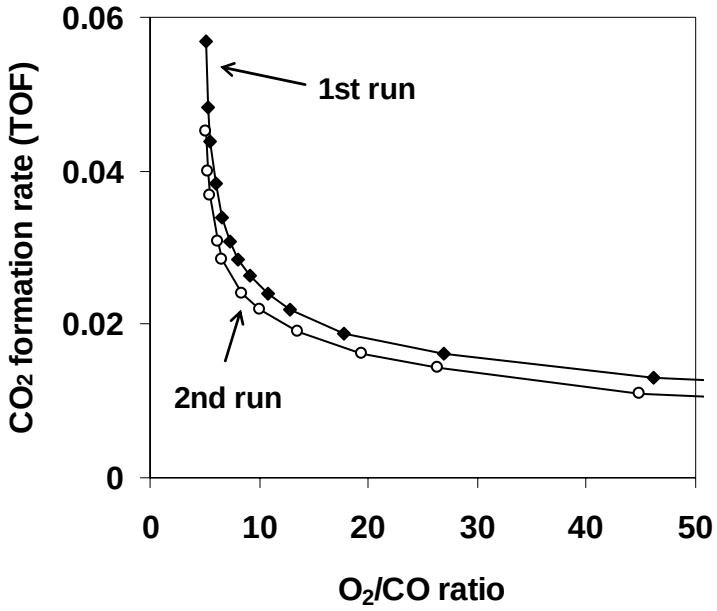

Fig. 40. CO_2 formation rate as a function of O_2/CO ratio for CO oxidation over an Au/TiO_2 reference catalyst at room temperature. The data were measured using 3 mg of Au/TiO_2 with an initial O_2/CO ratio of 2.

CHAPTER VI

SYNTHESIS OF WELL-ORDERED ULTRA-THIN TITANIUM OXIDE FILMS ON Mo(112)*

Introduction

Metal oxide surfaces have received increased interest due to their fundamental importance in applications such as heterogeneous catalysis, metal–ceramic interfaces, gas sensors, and solid-state electronic devices. Despite this, these surfaces have been studied to a much lesser extent than metals and semiconductors due to their insulating character. To obviate this problem, ordered oxide films have been successfully synthesized on conducting substrates recently [161-165], which increases the conductivity sufficiently to allow the application of electron spectroscopies and scanning tunneling microscopy (STM). This approach is especially significant for wide bandgap insulating oxides, such as SiO_2, where the ultra-thin films are conductive enough for study [166-170].

Among the various oxide systems, titanium dioxide has served as the prototypical reducible metal oxide for academic studies [171] based on its availability as a single crystal, easy preparation and semiconductivity, which makes it amenable to

* Reprinted from Surface Science, Vol 581, M.S. Chen, W.T. Wallace, D. Kumar, Z. Yan, K.K. Gath, Y. Cai, Y. Kuroda, and D.W. Goodman, Synthesis of well-ordered ultra-thin titanium oxide films on Mo(112), L115-L121, Copyright (2005), with permission from Elsevier; and reproduced in part with permission from "On the Origin of the Unique Properties of Supported Au Nanoparticles", M.S. Chen, Y. Cai, Z. Yan, and D.W. Goodman, *Journal of the American Chemical Society*, 2006, 128, 6341-6346. Copyright [2006] American Chemical Society.

surface science techniques. TiO_2 is also employed in a wealth of applications [172, 173]. Recently, thin TiO_2 films have been grown on various metal surfaces, such as Pt(111) [174], Mo(100) [175, 176], Mo(110) [177, 178], Ni(110) [179, 180], and W(100) [181].

Recently, a well-ordered monolayer titanium oxide film on the Mo(112) surface was prepared in our laboratories [182]. This TiO_x surface was found to be completely wetted by Au, forming well-ordered mono- and bilayer Au films. The bilayer Au structure exhibits unprecedented catalytic activity for CO oxidation [116]. In this chapter, the synthesis and characterization of this TiO_x film are described. In addition, the origin of the exceptionally high catalytic activity of the Au bilayer structure is discussed. Dr. Chen and I carried out the experiments in the HREELS chamber. The STM and XPS experiments were carried out in other surface analysis chambers by Dr. Wallace, Dr. Kumar, and K. Gath.

Experimental

The experiments were carried out in three separate ultra-high vacuum (UHV) chambers. One was equipped with a high-resolution electron energy loss spectroscopy (HREELS) with a base pressure of 2×10^{-10} Torr, one was equipped with a scanning tunneling microscopy (STM) at a base pressure of 2×10^{-9} Torr, and one was equipped with an X-ray photoelectron spectroscopy (XPS) with a base pressure of 8×10^{-10} Torr. The HREELS and STM chambers were also equipped with the basic surface science techniques of a cylindrical mirror analyzer for AES, low-energy electron diffraction (LEED), and a quadrupole mass analyzer. The Mo(112) sample was cleaned by repeated

cycles of oxidation at 1200 K followed by an anneal to 2100–2200 K, and characterized using AES and LEED. The substrate temperature was measured via a C-type thermocouple (W-5%Re/W-26%Re) spot-welded to the back of the crystal. A liquid-nitrogen cryostat and an electron beam heater allowed control of the sample temperature between 90 and 2300 K. The energy resolution of the HREELS measurements was between 64 and 96 cm^{-1} (8–12 meV) as determined by the full width at half-maximum (FWHM) of the elastic peak using a primary energy (E_p) of ~5 eV; the monochromatized electrons were incident at an angle of 60° with respect to the sample normal. The XPS spectra were collected using a Mg anode (1253.6 eV) and a precision PHI hemispherical analyzer operated with a pass energy of 58.7 eV in the fixed analyzer transmission mode. All binding energies were referenced to Mo $3d_{5/2}$ peak at 227.7 eV.

Au was deposited onto the Mo(112)-(8×2)-TiO_x surface from a Au wire wrapped around a Ta filament that was heated resistively. The surface was then annealed at 900 K in ~3×10^{-9} Torr O_2. The Au flux was calibrated using AES break points on Mo(112) and (8×2)-TiO_x/Mo(112). The Au coverage is reported in monolayers (ML) and referenced to the top layer Mo atom density in Mo(112). The order of the Au(1×1) and (1×3) structures were confirmed by sharp LEED patterns at Au coverages of ~1 and 1.3 ML, respectively.

Results and Discussion

To synthesize the TiO_x film, a well-ordered ultra-thin silica film was prepared first on the Mo(112) surface. The details of the preparation and characterization of this

silica film were reported previously [170]. In short, less than a monolayer (ML) of Si was deposited onto a Mo(112)–p(2×3)–O surface, and oxidized at 800 K in a 1×10^{-7} Torr O_2 for 5 min, followed by an increase in the substrate temperature to 1200 K for an additional 5 minutes. This procedure (depositing/oxidation/annealing) was repeated until a constant Si/Mo AES ratio was achieved. The resulting surface gave a sharp c(2×2) LEED pattern, as shown in Fig. 41A. Based on HREELS studies [170], the c(2×2) surface has been proposed to be a well-ordered Mo(112)–c(2×2)-[SiO_4] structure, where in each c(2×2) surface unit there is one [SiO_4] tetrahedron where all four oxygen atoms bind to Mo substrate atoms. The assumed surface structure was further confirmed by probe molecule adsorption in which benzene molecules adsorb essentially parallel with the surface up to the first three layers. This is due to the quasi-hexagonal arrangements of the surface oxygen atoms, where each hexagon can accommodate a benzene molecule [183].

Ti (1–1.5 ML) was then deposited onto this well-ordered ultra-thin SiO_2 surface from a Ti wire wrapped tantalum filament that was heated resistively. The coverage of Ti was estimated from the AES break point in the gradient obtained from stepwise deposition of Ti onto the Mo(112) surface following oxidation at 850 K in 5×10^{-8} Torr O_2, as shown in Fig. 42A. In these plots, a break point at 7 min was observed for both the Ti/Mo and O/Mo AES ratios, and an almost constant Ti/O ratio was found after the break point. This was taken as evidence of the completion of the first TiO_x monolayer. A typical HREEL spectrum for 1 ML Ti on Mo(112) after oxidation at 850 K is shown in Fig. 43A(f).

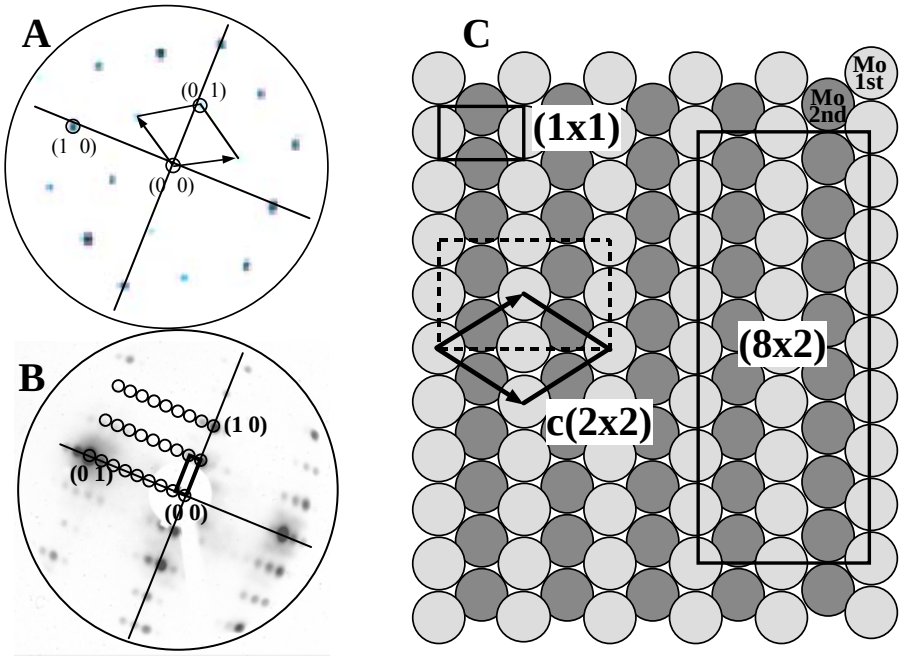

Fig. 41. (A) a c(2x2) LEED pattern for monolayer SiO_2 on Mo(112); (B) a (8x2) LEED pattern for monolayer TiO_x on Mo(112); (C) a top-view schematic of the clean Mo(112) surface. The solid lines show the primitive reciprocal and real unit cell.

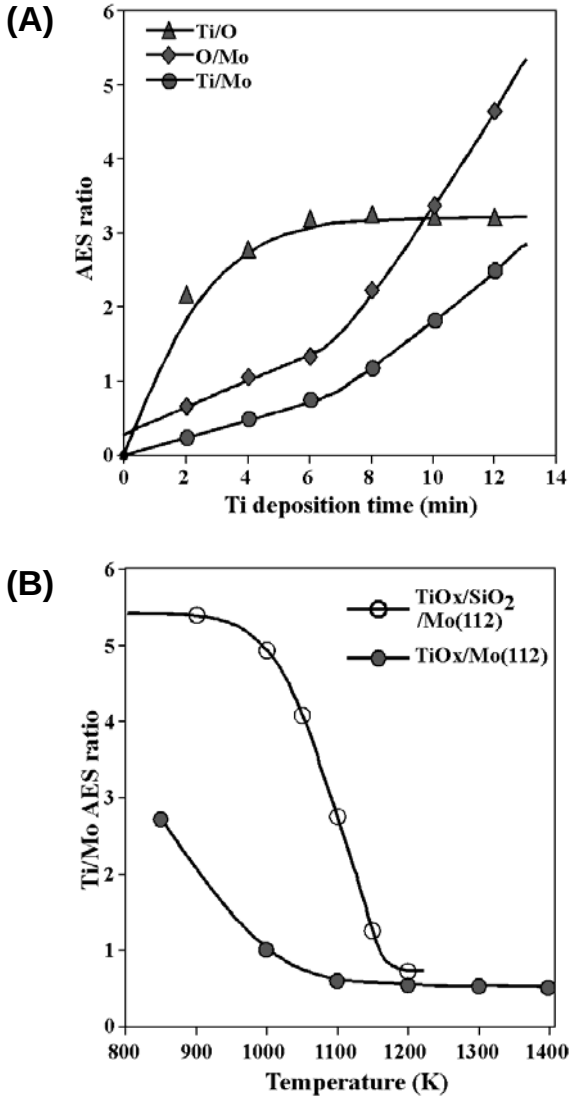

Fig. 42. AES ratios: (A) as a function of Ti deposition time for stepwise deposition of Ti onto Mo(112) following subsequent oxidation at 850 K on Mo(112); and (B) as a function of annealing temperature for TiO_x (2ML)/Mo(112) and TiO_x (~3 ML)/ SiO_2(monolayer)/Mo(112).

After depositing 1–1.5 ML Ti onto the SiO_2 surface, the sample was oxidized at 800 K in 5×10^{-8} Torr O_2 for 10 minutes. The corresponding HREEL and AES spectra are shown in Fig. 43. For comparison, spectra obtained after oxidizing at 600 K (Fig. 43A(b) and B(b)) are shown to illustrate the attenuation of Si and Mo AES lines and the Si–O phonon by the TiO_x overlayer. The details of the TiO_x–SiO_2 interface interactions were shown previously [184], where the formation of Si–O–Ti linkages were evidenced by a phonon peak at 127 eV, which is 4 eV lower than that at 131 eV for Si–O–Mo in HREELS; the change in the topmost surface from TiO_x to [SiO_4] was probed using benzene and H_2O adsorption. The sample was then annealed at 1200 K in 5×10^{-8} Torr O^2 for 10 minutes. The AES spectrum following this step (Fig. 43B(d)) showed that most of the SiO_2 was decomposed and desorbed, whereas an intense Si–O phonon in HREELS (Fig. 43A(d)) still existed due to the much stronger Si–O phonon intensity compared to Ti–O. A subsequent anneal at 1400 K in 1×10^{-8} O_2 for an additional 5 minutes completely removes the SiO_2 film and any residual Si based on the absence of a Si AES feature (see Fig. 43B(e)) and a Si–O phonon feature (Fig. 43A(e)). The TiO_x film exhibits a very sharp (8×2) LEED pattern (Fig. 41B), and a very smooth and well-ordered surface that exhibits relatively large terraces, as seen by STM images (Fig. 44A).

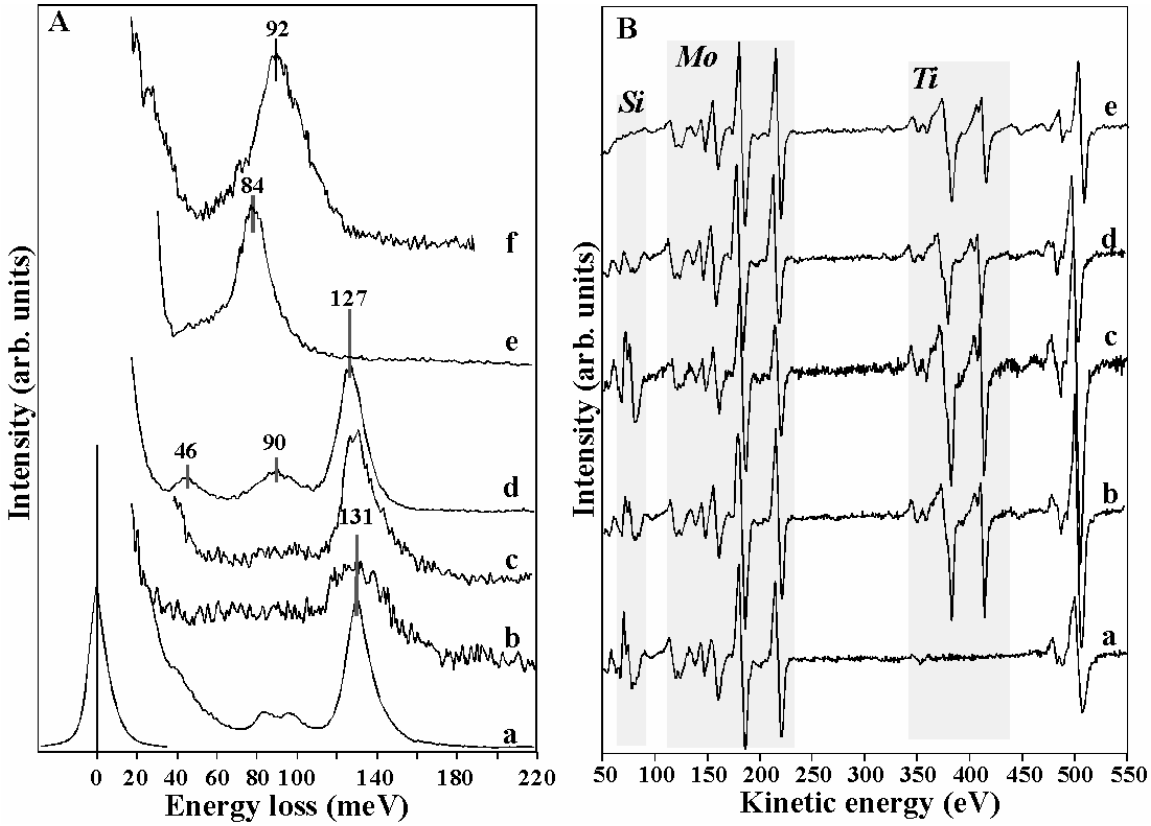

Fig. 43. (A) HREEL, and (B) AES spectra for 1.5 ML TiO_x on the SiO_2(monolayer)/Mo(112) surface following annealing at various temperatures: (a) SiO_2(monolayer)/Mo(112), (b) oxidized at 600 K, (c) oxidized at 800 K, (d) annealed at 1200 K, and (e) annealed at 1400 K, and (f) 1 ML Ti oxidized at 800 K.

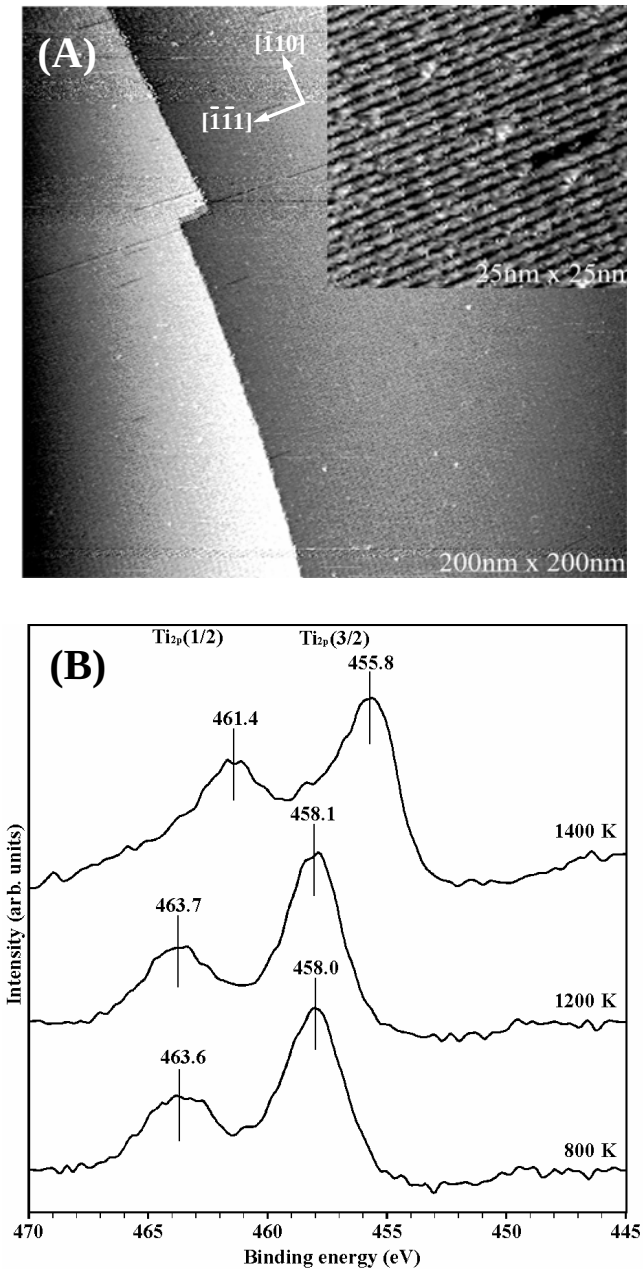

Fig. 44. (A) STM images of the obtained Mo(112)-(8x2)-TiO_x surface. $I = 0.18$ nA, $U_T = -1.7$ V (insert: $I = 0.18$ nA, $U_T = +1.2$ V); (B) XPS spectra for 1 ML Ti on Mo(112) following oxidation/annealing at indicated temperatures.

The thickness of this TiO_x film, determined using the AES intensity attenuation of the Mo MNN (187 eV), is estimated to be one-half of the electron inelastic mean free path (IMFP) for the TiO_x layer. The IMFP has been shown by Fuentes et al. [185] to be similar for various titanium compounds. A value of ~0.7 nm was obtained for both Ti and TiO_2 at 187 eV using the TPP-2M equation [185-191]. Assuming that the IMFP of TiO_x is close to that for Ti or TiO_2, a film thickness of ~0.35 nm for the TiO_x film can be derived, which corresponds to approximately 1 ML of TiO_2 or Ti_2O_3. The Ti/Mo AES ratio for a well-ordered (8×2)-TiO_x film is ~0.6, slightly lower than the 0.7 deduced from the break point in Fig. 42A. This difference could arise because of different surface structures and Ti oxidation states.

The (8×2)-TiO_x film can also be synthesized by the stepwise direct deposition of Ti onto an oxygen-covered Mo(112) surface, followed by subsequent oxidation–annealing cycles. However, the quality and reproducibility of the film derived from the direct deposition method are not comparable to that on a SiO_2 film. Fig. 42B shows a 2 ML Ti deposition on the Mo(112) surface following oxidation/annealing at various temperatures. Upon annealing this surface to 1100 K, the Ti/Mo AES ratio decreased rapidly to a value lower than the monolayer one of 0.6 (Fig. 42B). This surface requires a second or third deposition/oxidation/annealing cycle to achieve a saturation coverage and a sharp (8×2) LEED pattern. A similar behavior was observed for a ~3 ML TiO_x film on the monolayer SiO_2/Mo(112) surface (see Fig. 42B).

These results illustrate that the film syntheses are self-limiting in that different initial Ti coverages (1–2 ML) upon annealing lead to TiO_x films with identical Ti/Mo AES ratios corresponding to 1 ML and the same LEED pattern. The excess TiO_x may form three-dimensional (3-D) TiO_x clusters with lower AES and HREELS cross sections at medium annealing temperatures, and decompose/desorb at higher annealing temperatures. Furthermore, various Ti coverages, when annealed to 1400 K, show a single phonon feature at 84 meV related to the Ti–O stretching mode, consistent with the (8×2)-TiO_x structure found for 1 ML (Fig. 43A(e)). As illustrated on the monolayer SiO_2/Mo(112) surface [170], Ti–O–Mo or Ti–O–Ti species should exist for monolayer TiO_x/ Mo(112). Since the 84 meV single phonon feature is considerably lower than the 94–98 meV mode observed for bulk TiO_2 [177, 192] and ~102 meV mode for 3-D TiO_2 clusters observed on the Mo(112) surface when TiO_x/Mo(112) was annealed at 1000 K, the existence of Ti^{4+}–O–Ti^{4+} species was precluded. The mode at 84 meV likely originates from Ti^{3+}–O–Mo and/or Ti^{3+}–O–Ti^{3+}, or Ti^{4+}–O–Mo species, which are anticipated to have modes very near this value. To clarify the assignments of the 84 meV phonon feature, XPS was used to measure the oxidation states of Ti in the thin films. As displayed in Fig. 44B, ~1 ML Ti deposited on the Mo(112), followed by subsequent oxidation at 850 K, exhibits a Ti 2p(3/2) feature at a binding energy of approximately 458.0 eV, which is about 0.9 eV lower than 458.9 eV observed for multilayer TiO_2/Mo(112) [193]. As demonstrated previously for TiO_2/Mo(100) [176], the feature at 458.0 eV can be assigned to TiO_2(monolayer)/Mo(112). This assignment is consistent with a broad phonon feature in HREELS at approximately 92 meV (Fig.

43A(f)) and the coexistence of Ti^{4+}–O–Ti^{4+} (~95 meV) and Ti^{4+}–O–Mo (< 95 meV) species. Upon annealing to 1200 K in O_2, a shoulder at lower binding energy appears, and can be assigned to Ti in a lower oxidation state. With further annealing at 1400 K, the main peak shifts to 455.8 eV. This value is 2.2 eV lower than 458.0 eV for Ti^{4+} (Fig. 44B(a)) and very close to the difference (2 eV) between the binding energies of Ti^{3+} and Ti^{4+} [193, 194]. Thus, for the (8×2)-TiO_x film, it is likely that the oxidation state of Ti is most closely approximated as Ti^{3+}, with coexisting Ti^{3+}–O–Mo and Ti^{3+}–O–Ti^{3+} species that exhibit similar phonon features.

A row distance of 0.9 nm, corresponding to two rows of the Mo(112) trough along [–110] direction, is seen by STM (see Fig. 44A), consistent with the (8×2) LEED pattern observed (see Fig. 41). Since there are no observable *v*(CO) modes at 2130–2190 cm^{-1} [171, 195, 196] in infrared spectroscopy (IRAS) corresponding to $Ti^{\delta+}$–CO species for CO adsorption on this (8×2)-TiO_x at room temperature with CO pressures up to 100 Torr, there should be no surface dangling Ti bonds, or if so, these sites are inaccessible for CO molecules on the (8×2)-TiO_x surface. Thus, a possible structural model for the Mo(112)–(8×2)-TiO_x surface is proposed, as shown in Fig. 45, in which seven Ti atoms decorate every eight Mo atoms in the Mo(11 2) trough (the [–1–11] direction), and are bound to the surface via Ti–O–Mo bonds and to each other via Ti–O–Ti linkages.

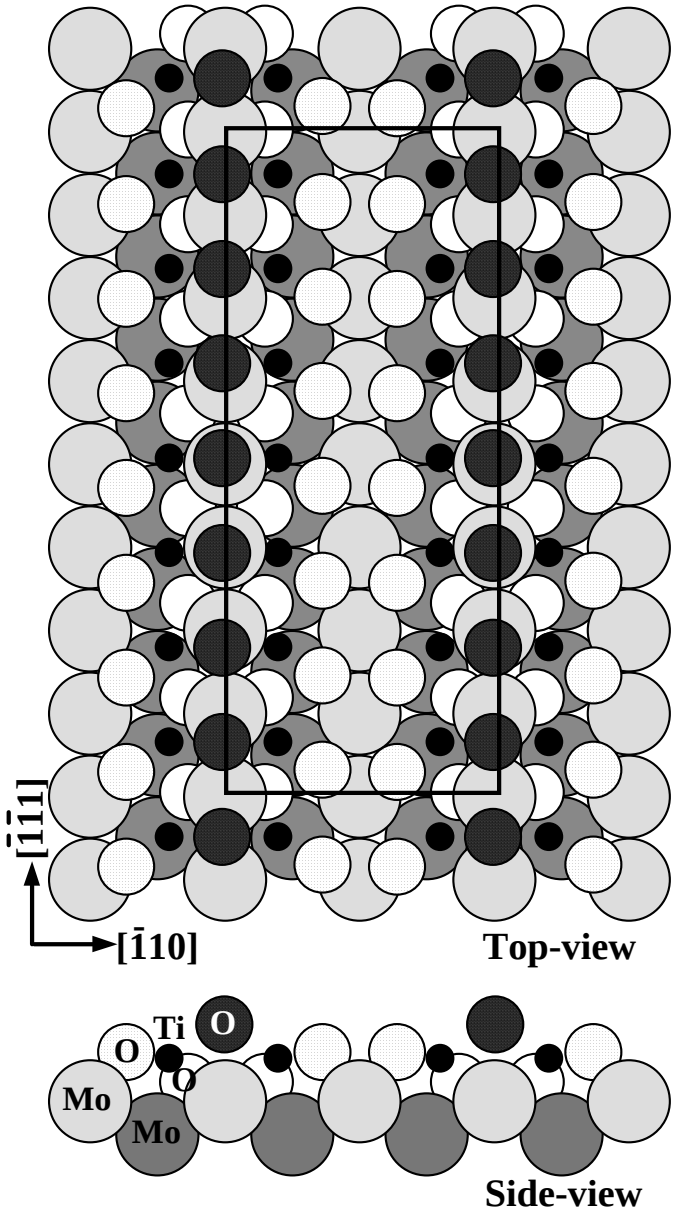

Fig. 45. Top- and side- view of a possible structural model for the Mo(112)-(8x2)-TiO_x.

Upon Au deposition onto this (8×2)-TiO_x surface and an anneal at 900 K, two well-ordered (1×1)-(Au,TiO_x) monolayer and (1×3)-(Au, TiO_x) bilayer structures form in which Au completely wets the titanium oxide surface [116]. A plot of the Au/Mo AES ratio versus deposition time, as well as the structural model of the (1×1)-Au/Mo(112), are shown in Fig. 46. Unprecedented catalytic activity for CO oxidation was observed for the Au bilayer structure [116]. The electronic and chemical properties of the ordered Au films have been studied in our laboratories [197].

A unique feature of supported Au catalysts is a sharp particle size dependence of the catalytic properties [6, 9, 198, 199]. From current-voltage (I-V) measurements of scanning tunneling spectroscopy (STS) on Au nanoparticles with various sizes on TiO_2(110), a metal-to-nonmetal transition (band gap variations between 0 and 1.4 eV) is observed as the Au cluster size is reduced from 3.5 to 1.0 nm (from a 3D multilayer to a 2D monolayer); a band gap of 0.2-0.6 V was found for Au bilayer nanoparticles [9]. A similar band gap-particle size relation has also been reported for Pd on TiO_2(110) [200]. Based on the variation of the band gap as a function of the particle size [9] and the significant difference of the valence band structure of the ordered Au thin films on TiO_x/Mo(112) compared with bulk Au, early work in our laboratories concluded that the pronounced structure sensitivity of CO oxidation on Au/TiO_2 relates directly to limited size or quantum size effects.

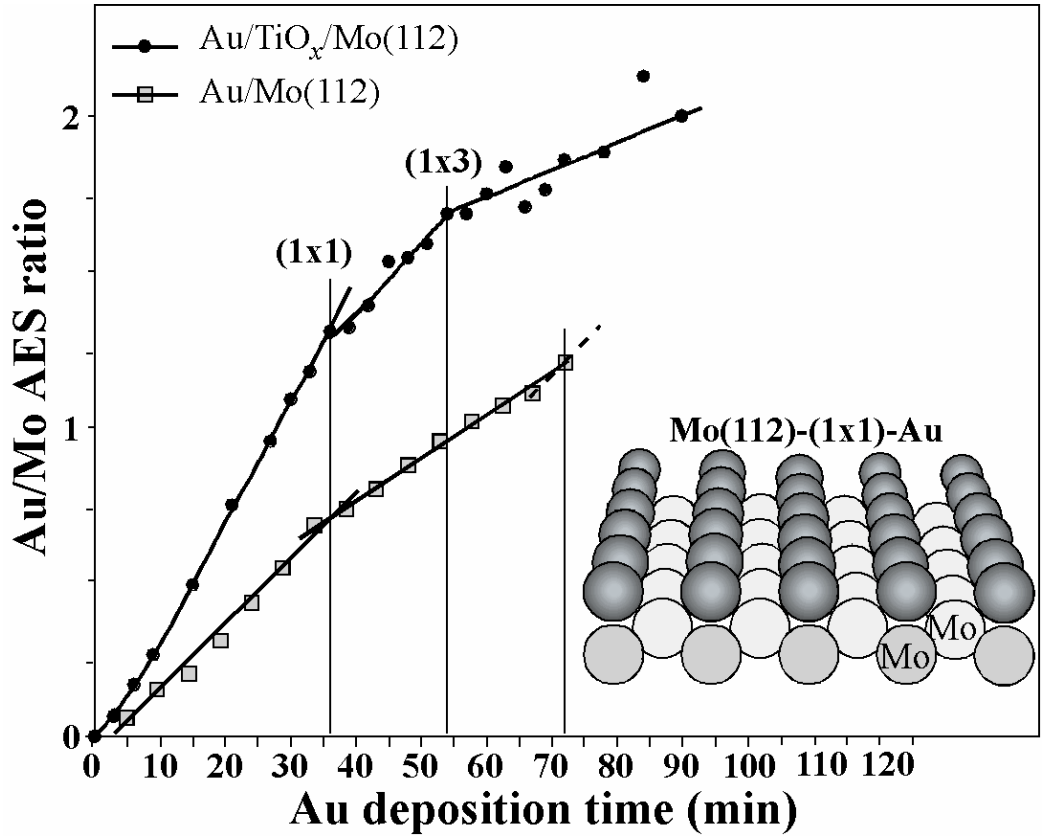

Fig. 46. Plots of Au/Mo AES ratios versus deposition time. The insert is a structural model of (1×1)-Au/Mo(112).

Limited size or quantum size effects have been invoked to account for the unique properties of nanometer-scale metallic particles relative to the bulk [201-203]. The properties of small metallic particles have been predicted theoretically to depend sensitively on the number of electrons, i.e., even or odd [204], manifested as tunneling between discrete electronic levels of single metal particles [205]. Quantum size effects, including electron transfer at the interface between Au nanoparticles and an oxide support, have been reviewed by Daniel et al. [151] and Chen [206]. Ag nanoparticles have been theoretically shown to exhibit three novel, size-dependent vibrational features compared to the bulk [207]. Conductance measurements on single Ag nanoparticles on Al_2O_3/NiAl(110) reveal a series of equidistant resonances near the Fermi level, with a decreasing energy separation with increasing cluster size [208]. Novel quantized charge transfer is manifested by a series of discrete features with uneven spacings and a relatively large band gap for small Au nanoparticles (< 1.6 nm) [206]. Significant quantum size effects with respect to the electronic configuration and the vibrational modes were found for Au nanoparticles less than 4 nm using Au-197 Mossbauer spectroscopy [209]. Ligand-stabilized metal nanoclusters in the size range of 1–2 nm exhibit well pronounced quantum size behavior [210]. Quantum well states in 1-D atomic chains of Au and/or Pd on NiAl(110) were found to be aligned as free-electron-like bands [211].

Quantum-size effects were also found to influence the thermodynamic properties of metallic nanoparticles [212], the properties of superconductors [213], and chemisorptive properties of nanosized materials [117, 118, 214-218]. Charge transfer

for CO adsorption depends critically on the size of a Na quantum dot [218]. Particle size effects were found for CO adsorption on Au deposits supported on FeO(111) grown on Pt(111) [217] and for CO [214] and oxygen [215] on Au/TiO_2. Pronounced thickness-dependent variations in the oxidation rate induced by quantum-well states were observed for ordered films up to 15 atomic layers in thickness [219]. All these studies indicate significant quantum size effects on the electronic, chemical, and catalytic properties of metal nanoparticles.

Based on theoretical [117, 118, 216, 220-222] and experimental studies [223, 224], low-coordination Au sites have been proposed to play a key role in defining the catalytic activity of Au nanoparticles. DFT calculations for small Au clusters by Metiu et al. showed that surface roughness rather than a band gap is more important in influencing the binding strength of CO to Au [216, 220]. TPD and IR results for CO adsorption on Au vapor-deposited on a thin FeO(111) film grown on a Pt(111) by Freund et al. indicate that the adsorption of CO is dependent primarily on cluster morphology [224]. This group attributed the observed particle size effects to the presence of highly uncoordinated Au atoms in very small particles rather than quantum size effects [217].

Kinetic measurements on Au monolayer and bilayer structures on $TiO_x/Mo(112)$ show that the Au bilayer is significantly more active than monolayer Au for CO oxidation at room temperature [116]. A comparison of the structures of the monolayer and bilayer structures reveals that the top layer Au atoms in each structure have very similar low coordination geometries. The relatively low activity of the monolayer

compared to the bilayer suggests that low coordinated sites in themselves are insufficient for enhanced catalytic activity for CO oxidation. The key to activity is the formation of a bilayer Au structure where charge polarization at the metal-oxide interface yields an electron-rich lower Au layer and a low-coordinated upper Au layer.

Clearly the support plays a key role in determining the unique catalytic activities of nanosized Au. The support stabilizes and defines the morphologies and electronic properties of Au nanoparticles [9, 50, 115-117, 215, 225]. The perimeter/contact area of the interface between the Au particles and the support has been proposed as a unique reaction site where reactants are activated [226-230]. The structural models of the two ordered Au monolayer and bilayer structures shown in Figure 5 show that the Ti^{n+} sites in TiO_x/Mo(112) are not assessable to the reactants, since each surface Ti site binds directly to a Au atom. The exceptionally high catalytic activities for CO oxidation observed on the ordered Au bilayer are more consistent then with a Au-only mechanism for CO oxidation. It should be noted, however, that under realistic catalytic reaction conditions, these ordered surfaces may restructure, exposing the TiO_x substrate to the reactants. Further in situ structural studies are required to address this critical question. In any case, an Au-only CO oxidation reaction pathway was recently shown by DFT calculations to have a similar activation energy (0.36–0.40 eV) as that involving the oxide support.

CHAPTER VII

SUMMARY

The catalytic oxidation of CO was studied over supported gold catalysts and various forms of Pt-group catalysts, including single crystals, polycrystalline metals, and supported catalysts.

A series of Au/TiO_2 catalysts were prepared from precursors of various metal-organic gold complexes (Au_n, n = 2–4) and their catalytic activity for CO oxidation was studied. The results showed that highly active Au/TiO_2 catalysts can be prepared from specific metal-organic gold complexes and a conventional TiO_2 support using the impregnation method. The catalytic activity and the particle size of the gold catalysts were strongly dependent on the gold complexes. The Au/TiO_2 catalyst prepared from a tetranuclear gold complex showed the best performance for CO oxidation with transmission electron microscopy of this catalyst indicating an average gold particle size of 3.1 nm. The catalysts also showed promising results for the PROX reaction.

The oxidation of CO was studied over Au/MgO catalysts, where the MgO supports were annealed to various temperatures between 900 and 1300 K prior to deposition of Au. A correlation was found between the activity of Au clusters for CO oxidation and the concentration of F-centers in the MgO support. These results were consistent with recent theoretical results showing that F-centers in MgO serve to anchor Au clusters and control their charge-state by partial transfer of charge from the substrate F-center to the Au cluster.

The oxidation of CO was studied in a batch reactor over supported Pd/Al_2O_3 catalysts, a Pd(100) single crystal, as well as polycrystalline metals of rhodium, palladium, and platinum. A hyperactive state, corresponding to an oxygen-covered surface, was observed at high O_2/CO ratios at elevated pressures. The reaction rate at this state was significantly higher than that on CO-covered surfaces at stoichiometric conditions. This behavior of Rh, Pd, and Pt is analogous to Ru, where the reaction rate increases by three orders of magnitude for the oxygen-covered surface compared to the clean Ru surface. The oxygen chemical potential (defined by the O_2/CO ratio) required to achieve the hyperactive state was found to closely depend on the intrinsic properties of the metal, the reaction temperature, and the particle size.

Well-ordered Mo(112)-(8x2)-TiO_x films were grown on the Mo(112) surface. Two preparation methods, direct growth on the Mo(112) surface and indirect growth by deposition of Ti onto monolayer SiO_2/Mo(112), were used. The latter method was more reproducible with respect to film quality as determined by low-energy electron diffraction and scanning tunneling microscopy. The thickness of this TiO_x film was one monolayer and the oxidation state of Ti was +3 as determined by Auger spectroscopy, high-resolution electron energy loss spectroscopy, and X-ray photoelectron spectroscopy.

REFERENCES

[1] G.C. Bond, P.A. Sermon, G. Webb, D.A. Buchanan, P.B. Wells, J. Chem. Soc., Chem. Commun. (1973) 444b.

[2] P.A. Sermon, G.C. Bond, P.B. Wells, J. Chem. Soc., Faraday Trans. I 75 (1979) 385.

[3] D.Y. Cha, G. Parravano, J. Catal. 18 (1970) 200.

[4] G. Cocco, S. Enzo, G. Fagherazzi, L. Schiffini, I.W. Bassi, G. Vlaic, S. Galvagno, G. Parravano, J. Phys. Chem. 83 (1979) 2527.

[5] J. Schwank, Gold Bulletin 16 (1983) 103.

[6] M. Haruta, N. Yamada, T. Kobayashi, S. Iijima, J. Catal. 115 (1989) 301.

[7] M. Haruta, S. Tsubota, T. Kobayashi, H. Kageyama, M.J. Genet, B. Delmo, J. Catal. 144 (1993) 175.

[8] G.R. Bamwenda, S. Tsubota, T. Nakamura, M. Haruta, Catal. Lett. 44 (1997) 83.

[9] M. Valden, X. Lai, D.W. Goodman, Science 281 (1998) 1647.

[10] M.M. Schubert, S. Hackenberg, A.C. van Veen, M. Muhler, V. Plzak, R.J. Behm, J. Catal. 197 (2001) 113.

[11] M. Haruta, Gold Bulletin 37 (2004) 27.

[12] S.H. Overbury, L. Ortiz-Soto, H. Zhu, B. Lee, M. Amiridis, S. Dai, Catal. Lett. 95 (2004) 99.

[13] M. Haruta, Catal. Today 36 (1997) 153.

[14] J. Guzman, B.C. Gates, Angew. Chem., Int. Ed. Engl. 42 (2003) 690.

[15] Y. Yuan, K. Asakura, H. Wan, K. Tsai, Y. Iwasawa, Chem. Lett. (1996) 755.

[16] Y. Yuan, A.P. Kozlova, K. Asakura, H. Wan, K. Tsai, Y. Iwasawa, J. Catal. 170 (1997) 191.

[17] A.P. Kozlova, S. Sugiyama, A.I. Kozlov, K. Asakura, Y. Iwasawa, J. Catal. 176 (1998) 426.

[18] Y. Yuan, K. Asakura, A.P. Kozlova, H. Wan, K. Tsai, Y. Iwasawa, Catal. Today 44 (1998) 333.

[19] A.P. Kozlova, A.I. Kozlov, S. Sugiyama, Y. Matsui, K. Asakura, Y. Iwasawa, J. Catal. 181 (1999) 37.

[20] T.V. Choudhary, C. Sivadinarayana, C.C. Chusuei, A.K. Datye, J.P. Fackler, Jr., D.W. Goodman, J. Catal. 207 (2002) 247.

[21] Z. Yan, S. Chinta, A.A. Mohamed, J.P. Fackler, D.W. Goodman, Catal. Lett. 111 (2006) 15.

[22] S.Y. Chin, O.S. Alexeev, M.D. Amiridis, Appl. Catal. A 286 (2005) 157.

[23] D.L. Trimm, Z.I. Önsan, Catal. Rev. -Sci. Eng. 43 (2001) 31

[24] M. Brown, A. Green, G. Cohn, H. Andersen, Ind. Eng. Chem. 52 (1960) 841.

[25] S.H. Oh, R.M. Sinkevitch, J. Catal. 142 (1993) 254.

[26] R.M.T. Sanchez, A. Ueda, K. Tanaka, M. Haruta, J. Catal. 168 (1997) 125.

[27] M.J. Kahlich, H.A. Gasteiger, R.J. Behm, J. Catal. 182 (1999) 430.

[28] G. Avgouropoulos, T. Ioannides, H.K. Matralis, J. Batista, S. Hocevar, Catal. Lett. 73 (2001) 33.

[29] G. Avgouropoulos, T. Ioannides, C. Papadopoulou, J. Batista, S. Hocevar, H.K. Matralis, Catal. Today 75 (2002) 157.

[30] R.J.D. Tilley, Principles and Applications of Chemical Defects, Stanley Thornes, Cheltenham, UK, 1998.

[31] A.M. Stoneham, Theory of Defects in Solids, Oxford University Press, Oxford, UK, 1975.

[32] S.L. Bernasek, W.J. Siekhaus, G.A. Somorjai, Phys. Rev. Lett. 30 (1973) 1202.

[33] V.E. Henrich, P.A. Cox, The Surface Science of Metal Oxides, Cambridge University Press, Cambridge, UK, 1994.

[34] E.A. Colbourn, Surf. Sci. Rep. 15 (1992) 281.

[35] K.E. Smith, J.L. Mackay, V.E. Henrich, Phys. Rev. B 35 (1987) 5822.

[36] G. Pacchioni, in: D.P. Woodruff (Ed.), The Chemical Physics of Solid Surfaces, Elsevier, Amsterdam, 2001.

[37] T.L. Thompson, J.T. Yates, Jr., Top. Catal. 35 (2005) 197.

[38] D.M. Murphy, R.D. Farley, I.J. Purnell, C.C. Rowlands, A.R. Yacob, J. Phys. Chem. B 103 (1999) 1944.

[39] L. Ojamäe, C. Pisani, J. Chem. Phys. 109 (1998) 10984.

[40] M. Sterrer, O. Diwald, E. Knözinger, J. Phys. Chem. B 104 (2000) 3601.

[41] D. Domínguez-Ariza, C. Sousa, F. Illas, Phys. Rev. B: Condens. Matter 68 (2003) 054101.

[42] M. Sterrer, T. Berger, S. Stankic, O. Diwald, E. Knözinger, ChemPhysChem 5 (2004) 1695.

[43] G. Pacchioni, ChemPhysChem 4 (2003) 1041.

[44] G. Pacchioni, P. Pescarmona, Surf. Sci. 412-413 (1998) 657.

[45] E. Scorza, U. Birkenheuer, C. Pisani, J. Chem. Phys. 107 (1997) 9645.

[46] T. Ito, J.-X. Wang, C.-H. Lin, J.H. Lunsford, J. Am. Chem. Soc. 107 (1985) 5062.

[47] T. Tashiro, T. Ito, K. Toi, J. Chem. Soc., Faraday Trans. 86 (1990) 1139.

[48] B.K. Min, W.T. Wallace, A.K. Santra, D.W. Goodman, J. Phys. Chem. 108 (2004) 16339.

[49] B. Yoon, H. Häkkinen, U. Landman, A.S. Wörz, J.-M. Antonietti, S. Abbet, K. Judai, U. Heiz, Science 307 (2005) 403.

[50] E. Wahlström, N. Lopez, R. Schaub, P. Thostrup, A. Rønnau, C. Africh, E. Lægsgaard, J.K. Nørskov, F. Besenbacher, Phys. Rev. Lett. 90 (2003) 026101.

[51] A. Sanchez, S. Abbet, U. Heiz, W.-D. Schneider, H. Häkkinen, R.N. Barnett, U. Landman, J. Phys. Chem. A 103 (1999) 9573.

[52] W.A. Sibley, Y. Chen, Phys. Rev. 160 (1967) 712.

[53] M.-C. Wu, C.M. Truong, D.W. Goodman, Phys. Rev. B 46 (1992) 12688.

[54] Y. Chen, W.A. Sibley, F.D. Srygley, R.A. Weeks, E.B. Hensley, R.L. Kroes, J. Phys. Chem. Solids 29 (1968) 863.

[55] M. Sterrer, E. Fischbach, M. Heyde, N. Nilius, H.P. Rust, T. Risse, H.J. Freund, J. Phys. Chem. B 110 (2006) 8665.

[56] M. Sterrer, M. Heyde, M. Novicki, N. Nilius, T. Risse, H.P. Rust, G. Pacchioni, H.J. Freund, J. Phys. Chem. B 110 (2006) 46.

[57] Z. Yan, S. Chinta, A.A. Mohamed, J.P. Fackler, Jr., D.W. Goodman, J. Am. Chem. Soc. 127 (2005) 1604.

[58] G. Ertl, H. Knözinger, J. Weitkamp (Eds.), Handbook of Heterogeneous Catalysis, Wiley-VCH, Weinheim, Germany, 1997.

[59] G.W. Keulks, C.C. Chang, J. Phys. Chem. 74 (1970) 2590.

[60] Y.-F.Y. Yao, J. Catal. 28 (1973) 139.

[61] T. Engel, G. Ertl, Adv. Catal. 28 (1979) 1.

[62] T. Engel, G. Ertl, in: D.A. King, D.P. Woodruff (Eds.), The Chemical Physics of Solid Surfaces and Heterogeneous Catalysis, Elsevier, Amsterdam, The Netherlands, 1982, p. 73.

[63] P.J. Berlowitz, C.H.F. Peden, D.W. Goodman, J. Phys. Chem. 92 (1988) 5213.

[64] G. Ertl, P. Rau, Surf. Sci. 15 (1969) 443.

[65] T. Engel, G. Ertl, J. Chem. Phys. 69 (1978) 1267.

[66] S. Ladas, H. Poppa, M. Boudart, Surf. Sci. 102 (1981) 151.

[67] C.H.F. Peden, D.W. Goodman, J. Phys. Chem. 90 (1986) 1360.

[68] N.W. Cant, P.C. Hicks, B.S. Lennon, J. Catal. 54 (1978) 372.

[69] H.-I. Lee, J.M. White, J. Catal. 63 (1980) 261.

[70] H. Beusch, P. Fieguth, E. Wicke, Chemie Ingenieur Technik - CIT 44 (1972) 445.

[71] F. Schueth, B.E. Henry, L.D. Schmidt, Adv. Catal. 39 (1993) 51.

[72] R. Imbihl, Catal. Today 105 (2005) 206.

[73] R. Imbihl, G. Ertl, Chem. Rev. 95 (1995) 697.

[74] R. Imbihl, Prog. Surf. Sci. 44 (1993) 185.

[75] L.F. Razon, R.A. Schmitz, Catal. Rev. -Sci. Eng. 28 (1986) 89.

[76] M. Sheintuch, Catal Rev 15 (1977) 107.

[77] R. Imbihl, M.P. Cox, G. Ertl, J. Chem. Phys. 84 (1986) 3519.

[78] M. Eiswirth, G. Ertl, Surf. Sci. 177 (1986) 90.

[79] S. Ladas, R. Imbihl, G. Ertl, Surf. Sci. 198 (1988) 42.

[80] R.C. Yeates, J.E. Turner, A.J. Gellman, G.A. Somorjai, Surf. Sci. 149 (1985) 175.

[81] B.C. Sales, J.E. Turner, M.B. Maple, Surf. Sci. 114 (1982) 381.

[82] S. Ladas, R. Imbihl, G. Ertl, Surf. Sci. 219 (1989) 88.

[83] N. Hartmann, R. Imbihl, W. Vogel, Catal. Lett. 28 (1994) 373.

[84] T. Ressler, M. Hagelstein, U. Hatje, W. Metz, J. Phys. Chem. B 101 (1997) 6680.

[85] A.A. Mohamed, H.E. Abdou, M.D. Irwin, J.M. López-de-Luzuriaga, J.P. Fackler, J. Cluster Sci. 14 (2003) 253.

[86] A.A. Mohamed, J.M. López-de-Luzuriaga, J.P. Fackler, Jr., J. Cluster Sci. 14 (2002) 61.

[87] S.M. Vesecky, J. Paul, D.W. Goodman, J. Phys. Chem. 100 (1996) 15242.

[88] A.K. Datye, Q. Xu, K.C. Kharas, J.M. McCarty, Catal. Today 111 (2006) 59.

[89] Y.-S. Ho, C.-B. Wang, C.-T. Yeh, J. Mol. Catal. A: Chem. 112 (1996) 287.

[90] M. Haruta, CATTECH 6 (2002) 102.

[91] M. Okumura, S. Tsubota, M. Haruta, J. Mol. Catal. A: Chem. 199 (2003) 73.

[92] H.-S. Oh, J.H. Yang, C.K. Costello, Y.M. Wang, S.R. Bare, H.H. Kung, M.C. Kung, J. Catal. 210 (2002) 375.

[93] P. Broqvist, L.M. Molina, H. Grönbeck, B. Hammer, J. Catal. 227 (2004) 217.

[94] J.-D. Grunwaldt, C. Kiener, C. Wögerbauer, A. Baiker, J. Catal. 181 (1999) 223.

[95] S.D. Lin, M. Bollinger, M.A. Vannice, Catal. Lett. 17 (1993) 245.

[96] M. Okumura, K. Tanaka, A. Ueda, M. Haruta, Solid State Ionics 95 (1997) 143.

[97] Y. Iwasawa, Tailored Metal Catalysts, Reidel, Dordrecht, Holland, 1986.

[98] Y. Iwasawa, Adv. Catal. 35 (1987) 187.

[99] Y. Yuan, K. Asakura, H. Wan, K. Tsai, Y. Iwasawa, Catal. Lett. 42 (1996) 15.

[100] Y. Choi, H.G. Stenger, J. Power Sources 129 (2004) 246.

[101] S. Kandoi, A.A. Gokhale, L.C. Grabow, J.A. Dumesic, M. Mavrikakis, Catal. Lett. 93 (2004) 93.

[102] G.G. Xia, Y.G. Yin, W.S. Willis, J.Y. Wang, S.L. Suib, J. Catal. 185 (1999) 91.

[103] E. Gulari, C. Guldur, S. Srivannavit, S. Osuwan, Appl. Catal. A 182 (1999) 147.

[104] S. Imamura, H. Sawada, K. Uemura, S. Ishida, J. Catal. 109 (1988) 198.

[105] A.Q. Wang, C.M. Chang, C.Y. Mou, J. Phys. Chem. B 109 (2005) 18860.

[106] J.H. Liu, A.Q. Wang, Y.S. Chi, H.P. Lin, C.Y. Mou, J. Phys. Chem. B 109 (2005) 40.

[107] A.-Q. Wang, J.-H. Liu, S.D. Lin, T.-S. Lin, C.-Y. Mou, J. Catal. 233 (2005) 186.

[108] A.A. Mohamed, A. Burini, J.P. Fackler, Jr., J. Am. Chem. Soc. 127 (2005) 5012.

[109] A.A. Mohamed, R. Galassi, F. Papa, A. Burini, J.P. Fackler, Inorg. Chem. 45 (2006) 7770.

[110] Y. Chen, R.T. Williams, W.A. Sibley, Phys. Rev. 182 (1969) 960.

[111] G.P. Summers, T.M. Wilson, B.T. Jeffries, H.T. Tohver, Y. Chen, M.M. Abraham, Phys. Rev. B 27 (1983) 1283.

[112] M.-C. Wu, C.M. Truong, K. Coulter, D.W. Goodman, J. Am. Chem. Soc. 114 (1992) 7565.

[113] M.C. Wu, C.M. Truong, K. Coulter, D.W. Goodman, J. Catal. 140 (1993) 344.

[114] U. Heiz, A. Sanchez, S. Abbet, W.D. Schneider, Chem. Phys. 262 (2000) 189.

[115] J.A. Rodriguez, G. Liu, T. Jirsak, J. Hrbek, Z. Chang, J. Dvorak, A. Maiti, J. Am. Chem. Soc. 124 (2002) 5242.

[116] M.S. Chen, D.W. Goodman, Science 306 (2004) 252.

[117] N. Lopez, T.V.W. Janssens, B.S. Clausen, Y. Xu, M. Mavrikakis, T. Bligaard, J.K. Nørskov, J. Catal. 223 (2004) 232.

[118] N. Lopez, J.K. Nørskov, T.V.W. Janssens, A. Carlsson, A. Puig-Molina, B.S. Clausen, J.-D. Grunwaldt, J. Catal. 225 (2004) 86.

[119] E. Lundgren, G. Kresse, C. Klein, M. Borg, J.N. Andersen, M. De Santis, Y. Gauthier, C. Konvicka, M. Schmid, P. Varga, Phys. Rev. Lett. 88 (2002) 246103.

[120] G. Zheng, E.I. Altman, Surf. Sci. 504 (2002) 253.

[121] D. Zemlyanov, B. Aszalos-Kiss, E. Kleimenov, D. Teschner, S. Zafeiratos, M. Havecker, A. Knop-Gericke, R. Schlogl, H. Gabasch, W. Unterberger, K. Hayek, B. Klotzer, Surf. Sci. 600 (2006) 983.

[122] J. Szanyi, D.W. Goodman, J. Phys. Chem. 98 (1994) 2972.

[123] D.A. Logan, M.T. Paffett, J. Catal. 133 (1992) 179.

[124] C.T. Campbell, Phys. Rev. Lett. 96 (2006) 066106.

[125] Y. Cai, M.S. Chen, D.W. Goodman, In Situ PM-IRAS Investigations of CO Oxidation on Pd(110), unpublished work (2007).

[126] M. Salmeron, L. Brewer, G.A. Somorjai, Surf. Sci. 112 (1981) 207.

[127] R.A. Bennett, S. Poulston, I.Z. Jones, M. Bowker, Surf. Sci. 401 (1998) 72.

[128] J. Gustafson, A. Mikkelsen, M. Borg, J.N. Andersen, E. Lundgren, C. Klein, W. Hofer, M. Schmid, P. Varga, L. Kohler, G. Kresse, N. Kasper, A. Stierle, H. Dosch, Phys. Rev. B 71 (2005) 115442.

[129] A. Stierle, N. Kasper, H. Dosch, E. Lundgren, J. Gustafson, A. Mikkelsen, J.N. Andersen, J. Chem. Phys. 122 (2005) 044706.

[130] E.H. Voogt, A.J.M. Mens, O.L.J. Gijzeman, J.W. Geus, Surf. Sci. 373 (1997) 210.

[131] M. Todorova, E. Lundgren, V. Blum, A. Mikkelsen, S. Gray, J. Gustafson, M. Borg, J. Rogal, K. Reuter, J.N. Andersen, M. Scheffler, Surf. Sci. 541 (2003) 101.

[132] T.W. Orent, S.D. Bader, Surf. Sci. 115 (1982) 323.

[133] J. Rogal, K. Reuter, M. Scheffler, Phys. Rev. Lett. 98 (2007) 046101.

[134] N.W. Cant, D.E. Angove, J. Catal. 97 (1986) 36.

[135] I.Z. Jones, R.A. Bennett, M. Bowker, Surf. Sci. 439 (1999) 235.

[136] J. Liu, M. Xu, F. Zaera, Catal. Lett. 37 (1996) 9.

[137] C.H.F. Peden, D.W. Goodman, M.D. Weisel, F.M. Hoffmann, Surf. Sci. 253 (1991) 44.

[138] Y. Cai, M.S. Chen, D.W. Goodman. to be published.

[139] T. Matsushima, D.B. Almy, D.C. Foyt, J.S. Close, J.M. White, J. Catal. 39 (1975) 277.

[140] T. Matsushima, J.M. White, J. Catal. 39 (1975) 265.

[141] T. Schalow, B. Brandt, M. Laurin, S. Schauermann, J. Libuda, H.J. Freund, J. Catal. 242 (2006) 58.

[142] T.E. Madey, H. Albert Engelhardt, D. Menzel, Surf. Sci. 48 (1975) 304.

[143] P.A. Thiel, J.T. Yates, W.H. Weinberg, Surf. Sci. 82 (1979) 22.

[144] H. Conrad, G. Ertl, J. Kuppers, E.E. Latta, Surf. Sci. 65 (1977) 245.

[145] N.A. Saliba, Y.L. Tsai, C. Panja, B.E. Koel, Surf. Sci. 419 (1999) 79.

[146] T.E. Madey, D. Menzel, Jpn. J. Appl. Phys. Suppl. 2, Pt. 2 (1974) 229.

[147] D.G. Castner, B.A. Sexton, G.A. Somorjai, Surf. Sci. 71 (1978) 519.

[148] G. Ertl, M. Neumann, K.M. Streit, Surf. Sci. 64 (1977) 393.

[149] G.V. Samsonov (Ed.), The Oxide Handbook, IFI/Plenum, New York, 1982.

[150] D. Astruc, F. Lu, J.R. Aranzaes, Angew. Chem., Int. Ed. 44 (2005) 7852.

[151] M.-C. Daniel, D. Astruc, Chem. Rev. 104 (2004) 293.

[152] A.P. Alivisatos, Science 271 (1996) 933.

[153] V.P. Zhdanov, B. Kasemo, J. Catal. 170 (1997) 377.

[154] S. Penner, P. Bera, S. Pedersen, L.T. Ngo, J.J.W. Harris, C.T. Campbell, J. Phys. Chem. B 110 (2006) 24577.

[155] T. Schalow, B. Brandt, D.E. Starr, M. Laurin, S.K. Shaikhutdinov, S. Schauermann, J. Libuda, H.J. Freund, Angew. Chem., Int. Ed. 45 (2006) 3693.

[156] T. Schalow, B. Brandt, M. Laurin, S. Schauermann, S. Guimond, H. Kuhlenbeck, J. Libuda, H.J. Freund, Surf. Sci. 600 (2006) 2528.

[157] J. Guzman, B.C. Gates, J. Am. Chem. Soc. 126 (2004) 2672.

[158] G.J. Hutchings, M.S. Hall, A.F. Carley, P. Landon, B.E. Solsona, C.J. Kiely, A. Herzing, M. Makkee, J.A. Moulijn, A. Overweg, J.C. Fierro-Gonzalez, J. Guzman, B.C. Gates, J. Catal. 242 (2006) 71.

[159] S. Minicò, S. Scirè, C. Crisafulli, A.M. Visco, S. Galvagno, Catal. Lett. 47 (1997) 273.

[160] L. Fu, N.Q. Wu, J.H. Yang, F. Qu, D.L. Johnson, M.C. Kung, H.H. Kung, V.P. Dravid, J. Phys. Chem. B 109 (2005) 3704.

[161] D.W. Goodman, Surf. Rev. Lett. 2 (1995) 9.

[162] C.T. Campbell, Surf. Sci. Rep. 27 (1997) 1.

[163] R. Franchy, Surf. Sci. Rep. 38 (2000) 195.

[164] S.A. Chambers, Surf. Sci. Rep. 39 (2000) 105.

[165] S.C. Street, C. Xu, D.W. Goodman, Annu. Rev. Phys. Chem. 48 (1997) 43.

[166] R.M. Jaeger, H. Kuhlenbeck, H.J. Freund, M. Wuttig, W. Hoffmann, R. Franchy, H. Ibach, Surf. Sci. 259 (1991) 235.

[167] Y.D. Kim, T. Wei, D.W. Goodman, Langmuir 19 (2003) 354.

[168] S. Wendt, Y.D. Kim, D.W. Goodman, Prog. Surf. Sci. 74 (2003) 141.

[169] T. Schroeder, J.B. Giorgi, M. Bäumer, H.J. Freund, Phys. Rev. B 66 (2002) 165422.

[170] M.S. Chen, A.K. Santra, D.W. Goodman, Phys. Rev. B: Condens. Matter 69 (2004) 155404.

[171] U. Diebold, Surf. Sci. Rep. 48 (2003) 53.

[172] A.L. Linsebigler, G. Lu, J.T. Yates, Chem. Rev. 95 (1995) 735.

[173] D. Panayotov, J.T. Yates, J. Phys. Chem. B 107 (2003) 10560.

[174] A.B. Boffa, H.C. Galloway, P.W. Jacobs, J.J. Benitez, J.D. Batteas, M. Salmeron, A.T. Bell, G.A. Somorjai, Surf. Sci. 326 (1995) 80.

[175] G.S. Herman, M.C. Gallagher, S.A. Joyce, C.H.F. Peden, J. Vac. Sci. Technol. B 14 (1996) 1126.

[176] W.S. Oh, C. Xu, D.Y. Kim, D.W. Goodman, J. Vac. Sci. Technol. A 15 (1997) 1710.

[177] Q. Guo, W.S. Oh, D.W. Goodman, Surf. Sci. 437 (1999) 49.

[178] X. Lai, Q. Guo, B.K. Min, D.W. Goodman, Surf. Sci. 487 (2001) 1.

[179] T.V. Ashworth, G. Thornton, Thin Solid Films 400 (2001) 43.

[180] Z. Chang, G. Thornton, Surf. Sci. 462 (2000) 68.

[181] N.D. McCavish, R.A. Bennett, Surf. Sci. 546 (2003) 47.

[182] M.S. Chen, W.T. Wallace, D. Kumar, Z. Yan, K.K. Gath, Y. Cai, Y. Kuroda, D.W. Goodman, Surf. Sci. 581 (2005) L115.

[183] M.S. Chen, A.K. Santra, D.W. Goodman, J. Phys. Chem. 108 (2004) 17940.

[184] M.S. Chen, D.W. Goodman, Surf. Sci. 574 (2005) 259.

[185] G.G. Fuentes, E. Elizalde, F. Yubero, J.M. Sanz, Surf. Interface Anal. 33 (2002) 230.

[186] S. Tanuma, C.J. Powell, D.R. Penn, Surf. Interface Anal. 11 (1988) 577.

[187] S. Tanuma, C.J. Powell, D.R. Penn, Surf. Interface Anal. 17 (1991) 911.

[188] S. Tanuma, C.J. Powell, D.R. Penn, Surf. Interface Anal. 17 (1991) 927.

[189] S. Tanuma, C.J. Powell, D.R. Penn, Surf. Interface Anal. 20 (1993) 77.

[190] S. Tanuma, C.J. Powell, D.R. Penn, Surf. Interface Anal. 21 (1994) 165.

[191] S. Tanuma, C.J. Powell, D.R. Penn, Surf. Interface Anal. 25 (1997) 25.

[192] G. Durinck, H. Poelman, P. Clauws, L. Fiermans, J. Vennik, G. Dalmai, Solid State Commun. 80 (1991) 579.

[193] D. Kumar, M.S. Chen, D.W. Goodman, Thin Solid Films 515 (2006) 1475.

[194] J.T. Mayer, U. Diebold, T.E. Madey, E. Garfunkel, J. Electron Spectrosc. Relat. Phenom. 73 (1995) 1.

[195] F. Boccuzzi, A. Chiorino, M. Manzoli, P. Lu, T. Akita, S. Ichikawa, M. Haruta, J. Catal. 202 (2001) 256.

[196] F. Boccuzzi, A. Chiorino, M. Manzoli, Surf. Sci. 502-503 (2002) 513.

[197] M.S. Chen, Y. Cai, Z. Yan, D.W. Goodman, J. Am. Chem. Soc. 128 (2006) 6341.

[198] M. Haruta, Chem. Rec. 3 (2003) 75.

[199] P. Claus, A. Bruckner, C. Mohr, H. Hofmeister, J. Am. Chem. Soc. 122 (2000) 11430.

[200] C. Xu, X. Lai, G.W. Zajac, D.W. Goodman, Phys. Rev. B: Condens. Matter 56 (1997) 13464.

[201] J.A.A.J. Perenboom, P. Wyder, F. Meier, Phys. Rep. 78 (1981) 173.

[202] W.P. Halperin, Rev. Mod. Phys. 58 (1986) 533.

[203] F.M. Mulder, T.A. Stegink, R.C. Theil, L.J. de Jongh, G. Schmid, Nature 367 (1994) 716.

[204] R. Kubo, J. Phys. Soc. Jpn. 17 (1962) 975.

[205] D.C. Ralph, C.T. Black, M. Tinkham, Phys. Rev. Lett. 74 (1995) 3241.

[206] S. Chen, J. Electroanal. Chem. 574 (2004) 153.

[207] A. Kara, T.S. Rahman, Phys. Rev. Lett. 81 (1998) 1453.

[208] N. Nilius, M. Kulawik, H.-P. Rust, H.-J. Freund, Surf. Sci. 572 (2004) 347.

[209] P.M. Paulus, A. Goossens, R.C. Thiel, A.M. van der Kraan, G. Schmid, L.J. de Jongh, Phys. Rev. B 64 (2001) 205418.

[210] G. Schmid, Adv. Eng. Mater. 3 (2001) 737.

[211] N. Nilius, T.M. Wallis, W. Ho, J. Phys. Chem. B 108 (2004) 14616.

[212] Y. Volokitin, J. Sinzig, L.J. de Jongh, G. Schmid, M.N. Vargaftik, I.I. Moiseevi, Nature 384 (1996) 621.

[213] Y. Guo, Y.-F. Zhang, X.-Y. Bao, T.-Z. Han, Z. Tang, L.-X. Zhang, W.-G. Zhu, E.G. Wang, Q. Niu, Z.Q. Qiu, J.-F. Jia, Z.-X. Zhao, Q.-K. Xue, Science 306 (2004) 1915.

[214] D.C. Meier, D.W. Goodman, J. Am. Chem. Soc. 126 (2004) 1892.

[215] V. Bondzie, S. Parker, C. Campbell, Catal. Lett. 63 (1999) 143.

[216] G. Mills, M.S. Gordon, H. Metiu, J. Chem. Phys. 118 (2003) 4198.

[217] C. Lemire, R. Meyer, S.K. Shaikhutdinov, H.J. Freund, Surf. Sci. 552 (2004) 27.

[218] V. Lindberg, B. Hellsing, J. Phys.: Condens. Matter 17 (2005) S1075.

[219] L. Aballe, A. Barinov, A. Locatelli, S. Heun, M. Kiskinova, Phys. Rev. Lett. 93 (2004) 196103.

[220] G. Mills, M. S.Gordon, H. Metiu, Chem. Phys. Lett. 359 (2002) 493.

[221] N. Lopez, J.K. Norskov, J. Am. Chem. Soc. 124 (2002) 11262.

[222] I.N. Remediakis, N. Lopez, J.K. Nørskov, Angew. Chem., Int. Ed. 44 (2005) 1824.

[223] C. Lemire, R. Meyer, S. Shaikhutdinov, H.-J. Freund, Angew. Chem., Int. Ed. Engl. 43 (2004) 118.

[224] S.K. Shaikhutdinov, R. Meyer, M. Naschitzki, M. Bäumer, H.J. Freund, Catal. Lett. 86 (2003) 211.

[225] C.C. Chusuei, X. Lai, K. Luo, D.W. Goodman, Top. Catal. 14 (2000) 71.

[226] M. Haruta, M. Date, Appl. Catal. A 222 (2001) 427.

[227] Z.-P. Liu, S.J. Jenkins, D.A. King, Phys. Rev. Lett. 94 (2005) 196102.

[228] L. Guczi, G. Peto, A. Beck, K. Frey, O. Geszti, G. Molnar, C. Daroczi, J. Am. Chem. Soc. 125 (2003) 4332.

[229] J.J. Pietron, R.M. Stroud, D.R. Rolison, Nano Lett. 2 (2002) 545.

[230] L.M. Molina, B. Hammer, Phys. Rev. Lett. 90 (2003) 206102.

VITA

Name: Zhen Yan

Address: Department of Chemistry
c/o Dr. D. Wayne Goodman
Texas A&M University
3255 TAMU
College Station, TX 77843-3255

Email Address: yanz18@hotmail.com

Education: Ph.D., Chemistry, Texas A&M University, 2007
M.S., Chemistry, Peking University, Beijing, China, 2002
B.S., Chemistry, Peking University, Beijing, China, 1999

Publications:

1) M.S. Chen, Y. Cai, Z. Yan, K.K. Gath, S. Axnanda, D.W. Goodman, "Highly Active Surfaces for CO Oxidation on Rh, Pd, and Pt", *Surf. Sci.* (2007) in press.

2) Z. Yan, S. Chinta, A.A. Mohamed, J.P. Fackler, Jr., D.W. Goodman, "CO Oxidation over Au/TiO_2 Prepared from Metal-Organic Gold Complexes", *Catal. Lett.* 111 (2006) 15.

3) M.S. Chen, Y. Cai, Z. Yan, D.W. Goodman, "On the Origin of the Unique Properties of Supported Au Bilayers", *J. Am. Chem. Soc.* 128 (2006) 6341.

4) Z. Yan, S. Chinta, A.A. Mohamed, J.P. Fackler, Jr., D.W. Goodman, "The Role of F-centers in Catalysis by Au Supported on MgO", *J. Am. Chem. Soc.* 127 (2005) 1604.

5) R.W.J. Scott, S. Chinta, O.M. Wilson, Z. Yan, D.W. Goodman, R.M. Crooks, "Titania-Supported PdAu Bimetallic Nanoparticles Prepared from Dendrimer-Encapsulated Nanoparticle Precursors", *J. Am. Chem. Soc.* 127 (2005) 1380.

6) M.S. Chen, W.T. Wallace, D. Kumar, Z. Yan, K.K. Gath, Y. Cai, Y. Kuroda, D.W. Goodman, "Synthesis of Well-Ordered Ultra-Thin Titanium Oxide Films on Mo(112)", *Surf. Sci.* 581 (2005) L115.

7) Y.-F. Han, J.-H. Wang, D. Kumar, Z. Yan, D.W. Goodman, "A Kinetic Study of Vinyl Acetate Synthesis over Pd-based Catalysts: Kinetics of Vinyl Acetate Synthesis over Pd–Au/SiO_2 and Pd/SiO_2 Catalysts", *J. Catal. 232* (2005) 467.